energies

MDPI

Article

A Novel Artificial Intelligence Maximum Power Point Tracking Technique for Integrated PV-WT-FC Frameworks

Mohammad Junaid Khan [1], Divesh Kumar [2], Yogendra Narayan [3], Hasmat Malik [4,*], Fausto Pedro García Márquez [5] and Carlos Quiterio Gómez Muñoz [6,*]

1 Department of Electrical and Electronics Engineering, Mewat Engineering College (Wakf), Nuh 122107, Haryana, India; mohammad.khan444@gmail.com
2 Department of Electronics & Communication Engineering, GLA University, Mathura 281406, Uttar Pradesh, India; divesh.kumar@gla.ac.in
3 Department of Electronics & Communication Engineering, Chandigarh University, Mohali 140413, Punjab, India; narayan.yogendra1986@gmail.com
4 BEARS, University Town, NUS Campus, Singapore 138602, Singapore
5 Ingenium Research Group, Business and Administration Department, Universidad Castilla-La Mancha, 13071 Ciudad Real, Spain; faustopedro.garcia@uclm.es
6 HCTLab Research Group, Electronics and Communications Technology Department, Universidad Autónoma de Madrid, 28049 Madrid, Spain
* Correspondence: hasmat.malik@gmail.com (H.M.); carlosq.gomez@uam.es (C.Q.G.M.)

Abstract: The development of each country depends on electricity. In this regard, conventional energy sources, e.g., diesel, petrol, etc., are decaying. Consequently, the investigations of renewable energy sources (RES) are increasing as alternate energy sources for the fulfillment of energy requirements. The output characteristics of RES are becoming non-linear. Therefore, the maximum power point tracking (MPPT) techniques are critical for extracting the maximum power point (MPP) from RES, e.g., photovoltaic (PV) and wind turbines (WT). RES such as the Fuel Cell (FC) has been hailed as one of the major capable RES for automobile applications since they continually create electricity for the dc-link (even if one or both RES are not supplied by solar and wind, the FC will continue to supply to the load). Adaptive Neuro-Fuzzy Inference System (AN-FIS) MPPT for PV, WT, FC, and Hybrid RES is employed in this research article to solve this problem. The high step-ups (boost converters) are connected with PV and FC modules, and the buck converter is connected with the WT framework, to extract the maximum amount of power using MPPT algorithms. The performance of proposed frameworks based on MPPT algorithms is assessed in variable operating conditions such as Solar-Radiation (SR), Wind-Speed (WS), and Hydrogen-Fuel-Rate (HFR). A novel AN-FIS MPPT framework has enhanced the power of Hybrid RES at DC-link, and also reduced the simulation time to reach the MPP when compared to the perturb and observe (P-&-O), Fuzzy-Logic Controller (F-LC), and artificial neural network (AN-N) MPPTs.

Keywords: artificial intelligence; maximum power point tracking; technique for integration; renewable energy sources; intelligent controller

Citation: Khan, M.J.; Kumar, D.; Narayan, Y.; Malik, H.; García Márquez, F.P.; Gómez Muñoz, C.Q. A Novel Artificial Intelligence Maximum Power Point Tracking Technique for Integrated PV-WT-FC Frameworks. *Energies* **2022**, *15*, 3352. https://doi.org/10.3390/en15093352

Academic Editor: Fernando Morgado-Dias

Received: 4 March 2022
Accepted: 26 April 2022
Published: 4 May 2022

1. Introduction

Due to alternate sources like PV, WT, and FC systems, they have recently become a unique core component in both isolated and grid-connected applications. When a RES is run at full power, it is more efficient and, therefore, MPPT can be employed. As the Power (P)/Voltage (V) and P/current (I) properties of PV cells and FCs are non-linear, numerous search approaches are commonly used [1]. However, when there are sudden variations in SR, humidity, or temperature, these methods can cause issues. In addition, there may be significant losses of power and incapacity to control partial shading conditions (PSC) in a PV framework. Multiple P-&-O MPPT has been proposed for the reversed buck–boost

dc–dc converter with parallel power processing and achieves the global MPP from solar PV frameworks under low SR and PSC. This work is simulated using MATLAB/SIMULINK and implemented in hardware [2]. The proposed work uses the relay circuit in order to achieve electrical reconfiguration to enhance the output power of the solar PV framework during PSC, using camera and MATLAB-Arduino interfacing [3]. Artificial intelligence MPPT approaches such as AN-N [4], F-LC, Genetic-Algorithm (GA), Differential-Evaluation (DE), Particle-Swarm-Optimization (PSO) [5], and Sliding-mode-control (SMC) [6] can be utilized to address these issues. The PV systems have been given additional exercises and complex organize mechanisms in favor of their assimilation into the power coordination, introducing an improved convene heuristic technique for decreasing fluctuations of power in the Hybrid RES [7]. It proposes a PV system allocation that considers both static and dynamic constraints [8]. WT is a promising technology, particularly in areas with strong WS. Getting the most electricity from WT is important in electrical power systems, hence control of these systems is a key topic to solve [9]. WT with MPPT is becoming more efficient and reliable due to artificial intelligence techniques. FC is also used to meet rising power demand in addition to these sources [10]. The hybrid RES plays a vital responsibility in power production in inaccessible regions where there is no availability of water [11]. Solar PV, WT, FC, and hybrid RES framework output power is influenced by SR, WS, HFR, load, and temperature of PV array [12]. To boost RES' performance, a high-power dc–dc converter is used [13]. Due to the SR, WS, and temperature all being dynamic, an MPPT controller is necessary to determine the RES's operating point [14]. The MPPT controller is used to get the most power out of PV, WT, FC, and hybrid RES systems [15]. Using an MPPT controller, it is possible to convert RES into electrical energy efficiently [16]. Researchers present a method for estimating the most likely PV power ramp rates (RR). The method's only inputs are the minimum PV system dimension and point irradiance and cloud shadow velocity observations. The proposed method was tested using 57 days of measured data from two PV systems. When compared to an existing approach that encircled the RR in the measured power 99.99 percent of the time, it performed better. The method can be applied to PV power plant design and component size [17]. Based on approximately 26,000 recorded current–voltage curves, this article gives an experimental analysis of the MPP characteristics of partially shaded strings of six and 17 series-connected solar modules, addressing the inadequacies of previous studies. The results show that by following the MPP nearest to the nominal MPP voltage at negligible energy losses, the large operating voltage range when the global MPP is followed can be greatly reduced. From 0.03 percent to 0.35 percent of available energy, the energy difference between the two MPPs was determined to be minimal [18]. Various MPPT techniques are described such as P-&-O [19], Incremental-Conductance (IN-C), and Artificial Intelligence (AI)-based MPPT techniques [20], e.g., F-LC, A-NN, and AN-FIS are producing the MPP. The simulation design and analysis of these MPPT techniques have been offered in this research. The PV, WT, FC and Hybrid RES with dc–dc converters, and the MPPT controllers are developed in MATLAB/SIMULINK platform. The MPPT technique used for a certain application is a critical design consideration. The efficiency, response time, peak overshoot, static and dynamic inaccuracy of the MPP tracker should all be considered, as should the sensors required, and the complexity of implementation. An AN-FIS MPPT model controls duty ratio in favor of power buck and boost converters, ensuring that the maximum power is given to the load (load can be resistive, inductive capacitive, etc.). The performance of proposed frameworks based on MPPT algorithms is assessed in variable operating conditions such as SR, WS, and HFR. In addition, the findings of the proposed MPPT system were compared to those obtained using the P-&-O, F-LC, and Artificial Neural-Network (AN-N) methods to assess its efficiency and performance of the tracking system. To compare various MPPT strategies, all of the above-mentioned considerations in favor of the MPPT framework were studied in the current research work.

The organization of this manuscript is arranged as follows: The P-&-O based MPPT is discussed in Section 2. Section 3 shows the MATLAB/SIMULINK based framework of

F-LC MPPT, together with its implementation and simulation analysis. Section 4 presents the MATLAB/SIMULINK based framework of the AN-N MPPT controller and its simulation analysis for changing in SR, WS, HFR and load resistance. In Section 5, the MATLAB/SIMULINK based model of the AN-FIS MPPT controller, along with its simulation analysis, has been discussed. Section 6 presents a comparative study of different MPPT techniques for diverse frameworks in MATLAB/SIMULINK, followed by a conclusion in Section 7.

2. P-&-O Based MPPT

The ratio of electrical power out (P_{out}) to SR, WS, and HFR input power (P_{in}) is the efficiency of the RES. The P_{out} of the MPPT controller must equal the maximum power (P_{max}). The most essential parameter of an MPPT algorithm is efficiency, which may be computed by Equation (1):

$$\eta_{MPPT} = \frac{\int_0^t P_{MPPT}(t)dt}{\int_0^t P_{max}(t)dt} \quad (1)$$

P_{MPPT} is the output power of RES using MPPT, while P_{max} denotes the maximum output power at actual MPP. MPPT's impact on the RES is determined by the following two variables:

(i) Static presentation (for a fixed MPP, how well it works).
(ii) Dynamic presentation (the degree to which it responds to changes in MPP).

The MPPT's accurateness in static and dynamic reveals how near PV, WT, FC frameworks are to MPP. PV module, for example, can be expressed as a percentage of ($I_{max} \times V_{max}$) or (P_{max}) [21] by Equation (2):

$$A_{MPPT} = \frac{X}{X_{max}} \quad (2)$$

where, X can be either I, V or P.

In this paper, the static and dynamic relative errors of the RES output power were investigated by Equations (3) and (4).

$$E_{MPPT,absolute} = |X - X_{max}| \quad (3)$$

$$E_{MPPT,relative} = \frac{X - X_{max}}{X_{max}} \quad (4)$$

From Figure 1, the system's Voltage [$V(k)$] and Current [$I(k)$] are measured in P-&-O, and the resultant power ($P_1 = P(k) = V(k)*I(k)$) is determined. The equivalent power [$P_2 = P(k-1) = V(k-1)*I(k-1)$] is then estimated by incorporating tiny perturbations of V (or duty-ratio "D") in favor of dc–dc power converter in the same track. Following that, the P_2 is compared to P_1. If $P_2 > P_1$, then the perturbation (ΔD) is in the right direction; otherwise, the perturbation's direction should be inverted. MPP is attained by using this method. Under steady-state conditions, the system will vary about the MPP. These oscillations are the source of energy loss and, as a result, a decreased efficiency. Figure 1 illustrates the flow chart of the P-&-O based MPPT controller [6]. Although P-&-O MPPT is simple and widely used in PV, WT, and FC RES, it has a key drawback in that it causes oscillation from the MPP when the environment changes rapidly. Correct perturbation size is required to obtain a good steady-state and dynamic response. Small perturbation sizes result in slow tracking performance, whereas large perturbation sizes result in substantial steady-state oscillations.

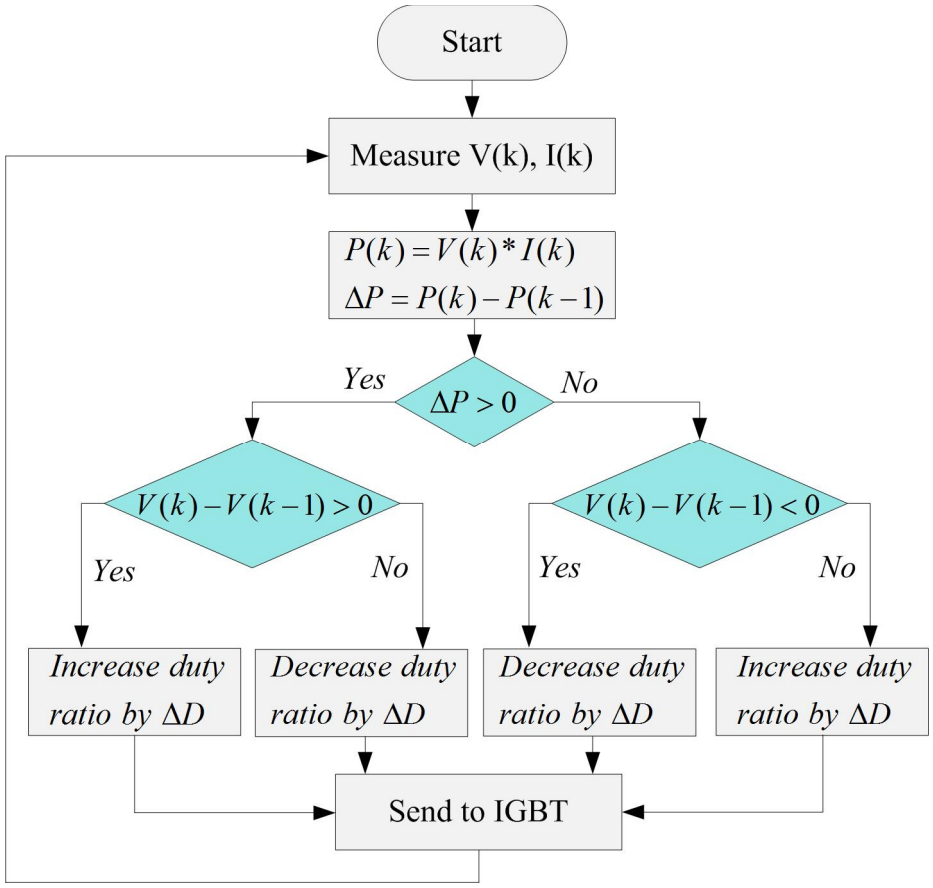

Figure 1. Flowchart of P-&-O based MPPT Algorithm.

Simulation Models Using P-&-O Based MPPT Technique

Specifications of the Vikram solar PV module and boost converter are given in Tables 1 and 2, respectively. PV framework consists of a dc–dc boost converter, load, and P-&-O based MPPT system. From Table 1, where V_{oc} represents the open-circuit voltage, I_{sc} represents the short circuit current, and V_{mp} & I_{mp} are the voltage and current at the MPP, respectively. TC stands for temperature coefficient, I_L represents the light generated current, I_o is the diode saturated current, q_e is the Electric charge, and n_s represents the series-connected cells in every array.

The MPP based on the P-&-O algorithm was computed by using the MATLAB/SIMULATION platform. For D computation, the algorithm receives voltage and current data. Figure 2 shows the change in SR test patterns used for simulation analysis. It has a 0.5-s step varying in SR from 800.0 to 600.0 W/m^2, with a 1-s ramp increase. As the ambient situation is never consistent, the test pattern for the PV framework simulation is a combination of step and ramp signals.

Tables 3 and 4 show the specifications for the WT base Induction Generator (WTIG) framework with buck converter. A model of a WT framework with a buck converter, load and P-&-O controller was created by SIMULINK.

Figure 3 shows the test pattern variation in WS, which was employed in the simulation analysis. It has a 0.5-s step varying in WS from 12 to 3.5 m/s, with a 1-s ramp increase.

Tables 2 and 5 show the specs of the Proton Exchange Membrane Fuel Cell (PEM-FC) framework with a simulated boost converter. The model of a PEM-FC framework consists of a boost converter, load, and P-&-O controller.

Table 1. Vikram Solar PV Array Technical Specifications.

Sr. No.	Technical Specification	Value
01	V_{oc} of PV Array	44 V
02	I_{sc} of PV Array	8.1 A
03	V_{mp} of PV Array	34.7 V
04	I_{mp} of PV Array	7.8 A
05	TC of V_{oc} (%/°C)	−0.36
06	TC of I_{sc} (%/°C)	0.025
07	I_L of PV Array	8.20 A
08	I_0 of PV Array	2.5×10^{-10} A
09	Ideality factor of a Diode	0.98
10	Shunt-resistance (R_p)	3126.56 Ω
11	Series-resistance (R_s)	0.52 Ω
12	q_e (coulombs)	1.6×10^{-19}
13	n_s	72
14	Series-connected arrays for every string (N_{ss})	2
15	Parallel-connected arrays for every string (N_{pp})	1
16	Boltzmann constant (k)	1.38×10^{-23}
17	Maximum power (in W)	270.66

Table 2. Specification of Boost Converter.

Sr. No.	Parameter	Value
01	Inductance (L)	3 mH
02	Capacitance (C_o)	470 µF
03	Switching-frequency (f_s)	100 KHz
04	Input-Voltage (V_{in})	88 V
05	Duty-ratio (D)	Depending on the input and output voltages of the system
06	Load resistance	100 Ohm (Ω)

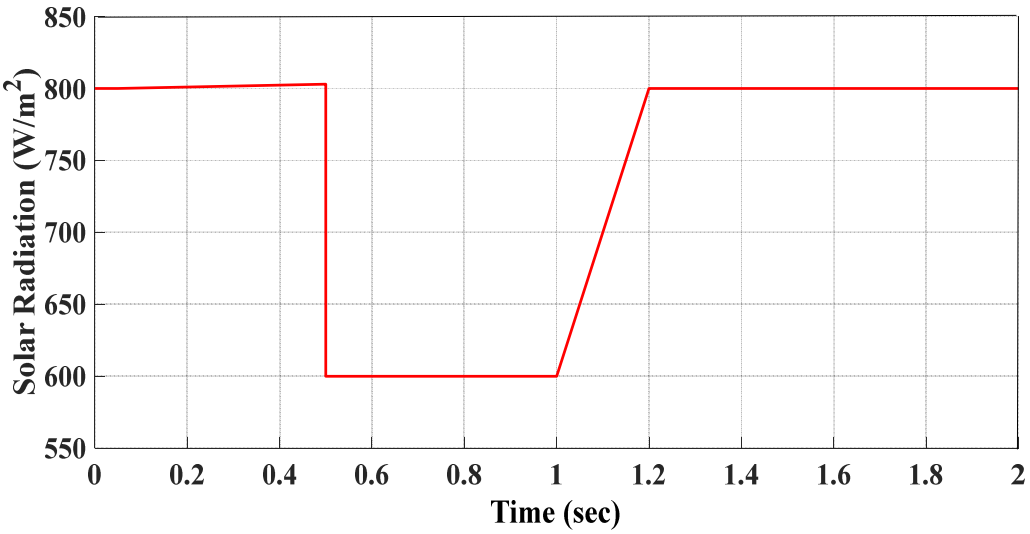

Figure 2. SR Test Pattern (in W/m^2) for Simulation Analysis.

Table 3. WTIG Module Specifications.

Sr. No.	Specification	Significance
01	Output Power (Nominal) of WT Framework	1200 W
02	Base WS (m/s)	12
03	Base rotation speed	1 pu
04	Maximum-pitch-angle	45 deg.
05	Maximum rate of change of pitch-angle	2 (deg./s)
	Induction Generator	
06	Nominal power of induction generator (in VA)	1200 (VA)
07	Line to line (L-to-L) voltage	415.0 (V_{rms})
08	Frequency (f) in Hz	50
09	Poles in Pairs	4.0
10	Constant of Inertia	5.04 0
11	Factor of Friction	0.010
	Three-Phase Programmable Voltage Source	
12	Positive-sequence (V_{rms} ph-ph)	25,000
13	Phase	0 deg.
14	Frequency	50 Hz
15	Load flow (generator type)	Swing
	Three-Phase Transformer	
16	Nominal power	100 W
17	Frequency	50 Hz
18	Voltage of winding 1	25,000 V
18	Voltage of winding 2	415 V
20	Magnetization resistance	500 (pu)
	Rectifier	
21	Used the Bridge arm	3
22	Snubber-resistance (R_S)	$1e^5$ Ohms
23	Snubber-capacitance (C_S)	Inf
24	Power electronic device	Diodes
25	Output-capacitor	1000 μF

Table 4. Specifications of Buck Converter.

Sr. No.	Specification	Significance
01	Inductor (L)	3 mH
02	Output Capacitor (C_0)	470 μF
03	Switching frequency (f_s)	10 kHz
04	Input Voltage (V)	300 V
05	Duty-ratio (D)	Varying
06	Load resistance	100 Ω

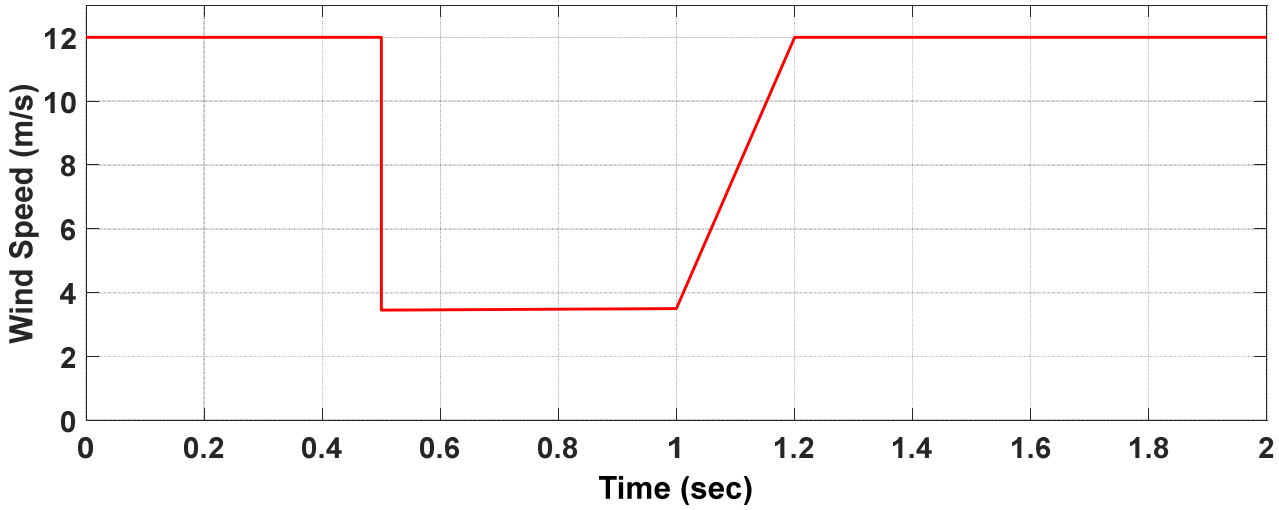

Figure 3. WS Test Pattern (in m/s) used for Simulation Analysis.

Table 5. Specifications of PEM-FC Module.

Sr. No.	Technical Specification	Value
01	Number of cells in a PEM-FC	48
02	Rated-power	1000 W
03	Performance in the form of voltage and current	28.8 V @ 35 A
04	[H_2] Supply valve-voltage	12 V
05	Purging valve voltage	12 V
06	Blower voltage	12 V
07	External temperature	5 to 30 °C
08	Maximum stack temperature	65 °C
09	Range of H_2 pressure (in bar)	0.45–0.55
10	Nominal stack efficiency	40%
11	Flow rate at max output	13 (lpm)
12	Hydrogen purity	99.995%
13	Shut-down (Low voltage)	24 V
14	Shut-down (Over current)	42 A
15	Shut-down (Over temperature)	65 °C

Similarly, the test patterns for HFR (in lpm) used Matlab/simulation testing, and is shown in Figure 4. It has a 0.5-s step varying in HFR from 13 to 12 lpm, with a 1-s ramp increase. The models of PV, WT and FC with a power converter and P-&-O controller are, in parallel, connected with a dc link (C_{dc} = 1000 µF) and resistive load. These models of PV, WTIG, PEM-FC systems with buck and boost converters and the hybrid system presented here, have been used for the analysis of P-&-O MPPT. A discrete power-guide simulation was run with a sampling time of 50 µs (i.e., 50 × 10^{-6} s), and an Ordinary –Differential-Equation (ODE-45) solver has been employed. The P-&-O MPPT controller was enabled at 0.10 s to offer enough start-up time for the PV, WT, FC, and hybrid RES outputs to stabilize. The Pulse-Width-Modulation (PWM) consists of a comparator and triangle waveform generating blocks whose frequency can be adjusted. In this paper, the test patterns of input deviation for PV, WT, and FC are shown in Figures 2–4, respectively.

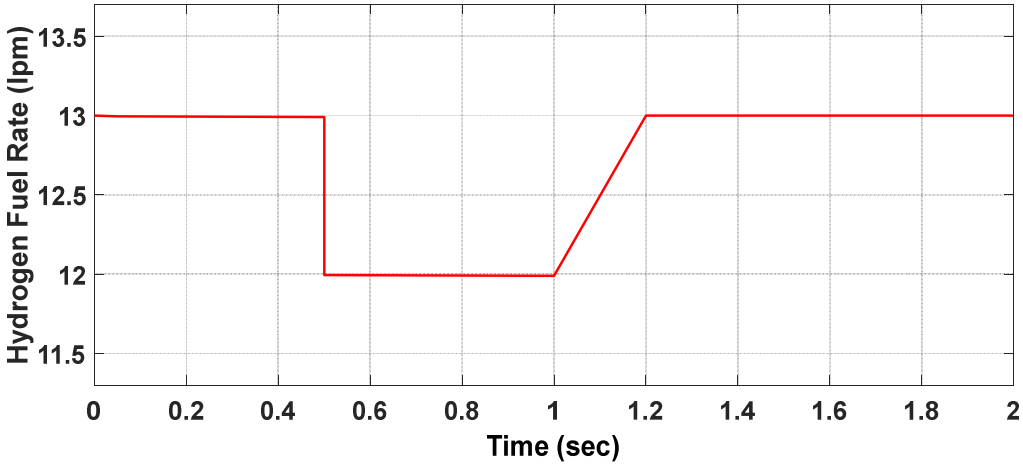

Figure 4. Test Pattern of HFR (lpm) used for Simulation Analysis.

Figures 5 and 6 show the input and output power, and the voltage of a boost converter with a PV system and P&O method. As the system's output is determined by the SR intensity, both waveforms have no distinct characteristics and may change when the SR intensity changes and result in a duty-ratio perturbation of 0.001. The circuit components cause the response to rise at first, and then it reacts to the input given to the PV array, as it is shown in Figure 2. Due to the P-&-O controller, there are fluctuations. Figures 7 and 8 show the input and output power and voltage of the buck converter with WTIG framework and P-&-O controller for variations in WS and a perturbation of duty-ratio (ΔD = 0.001). The output power and output voltage responses reveal an increase at the moment of 0.5 s, and a decrease at the instant of 1.2 s, according to the test input (Figure 3). Figures 9 and 10 show the input and output power and voltage of a boost converter with PEM-FC framework and a P-&-O controller for variations in HFR and a [ΔD = 0.001]. These responses also follow the test input (Figure 4) provided to the FC model, which is a step change until 1 s. A stable output is obtained after 3.5 s.

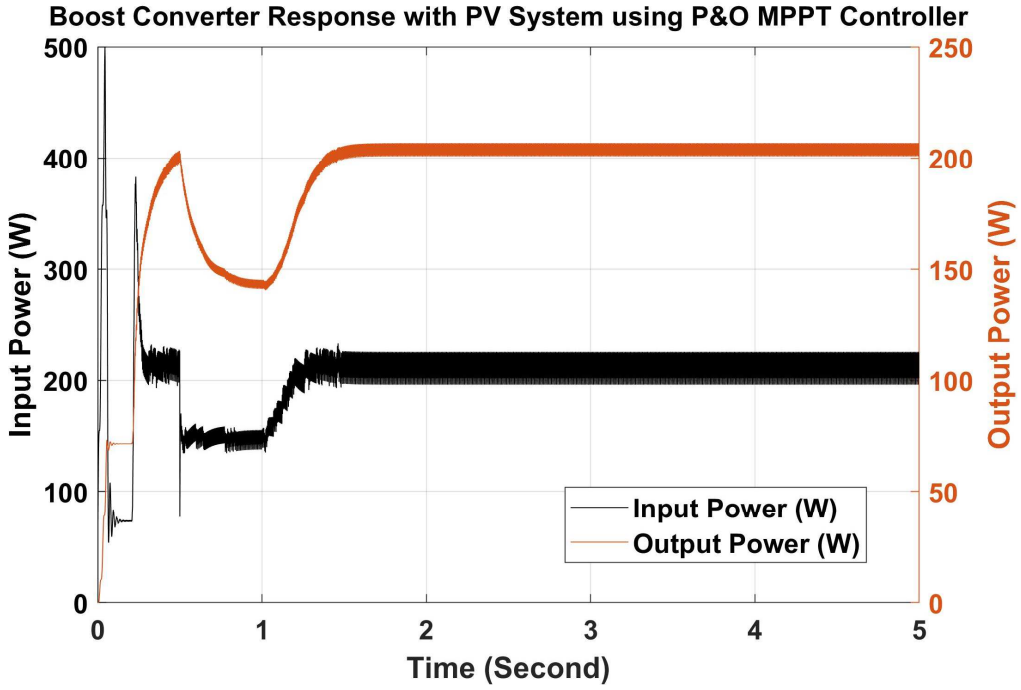

Figure 5. Input and Output Power of Boost Converter with PV System and P-&-O MPPT Controller.

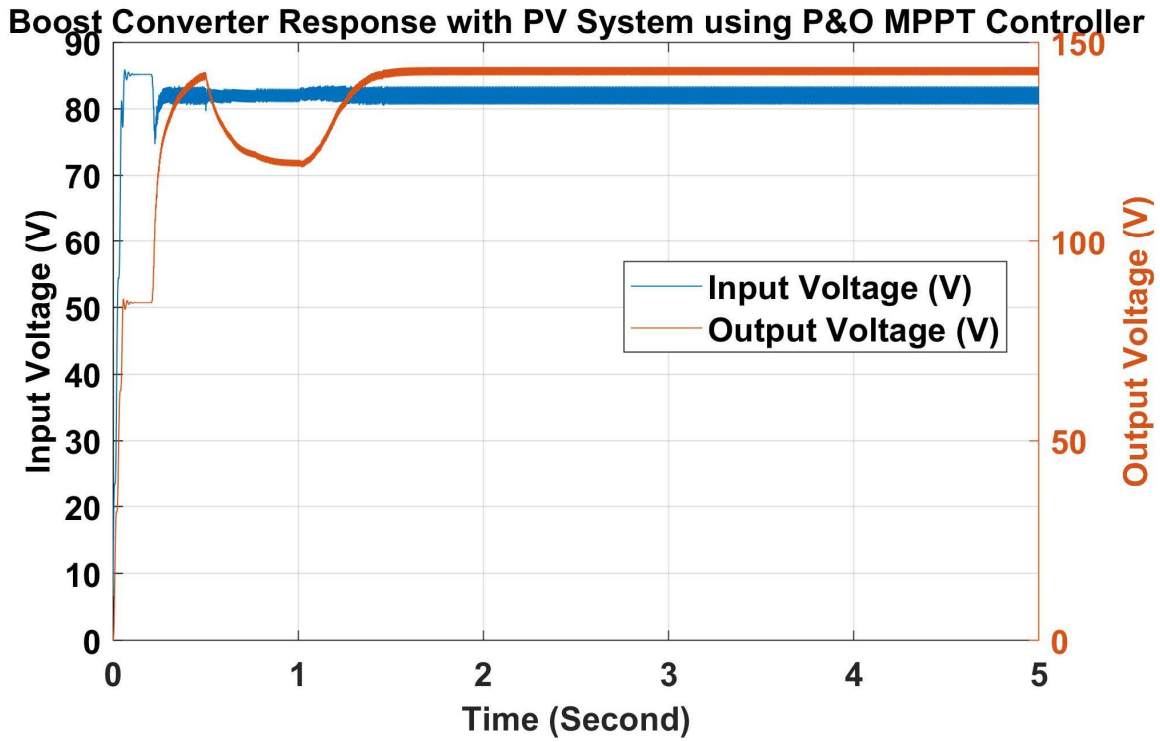

Figure 6. Input and Output Voltage of Boost Converter with PV System and P-&-O MPPT Controller.

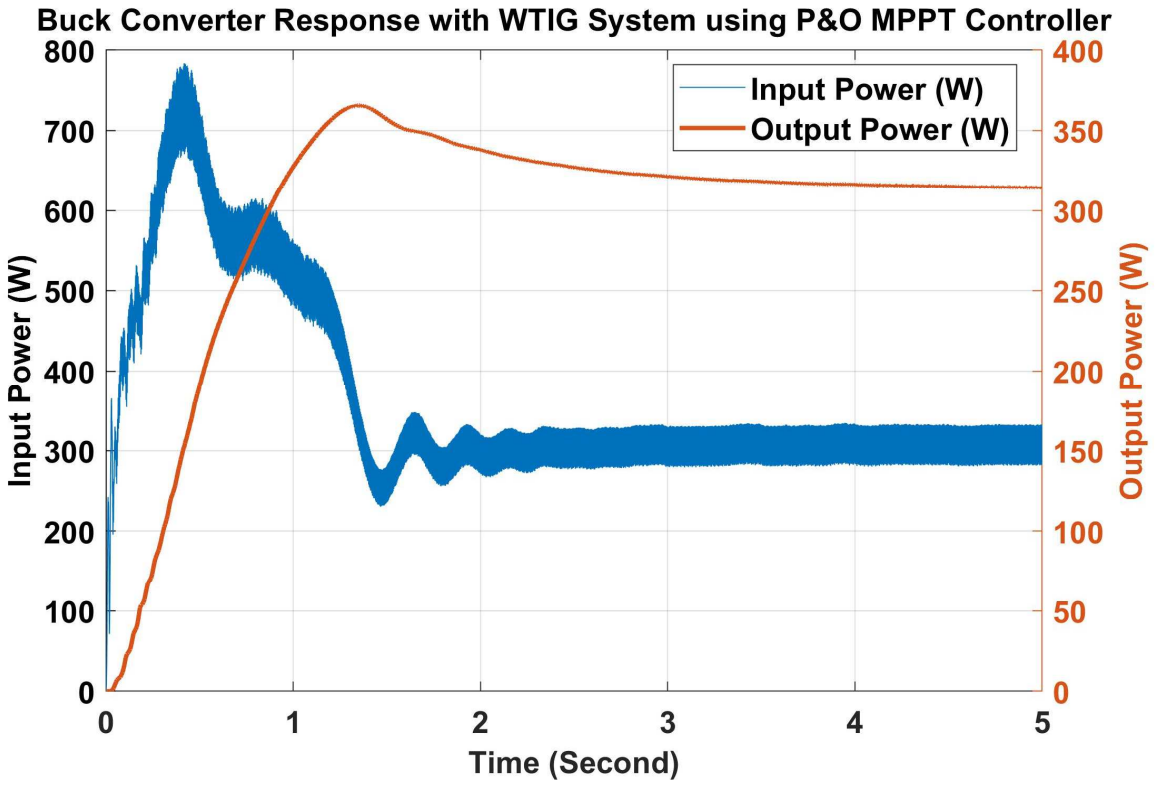

Figure 7. Input and Output Power of Buck Converter with WTIG System and P-&-O MPPT.

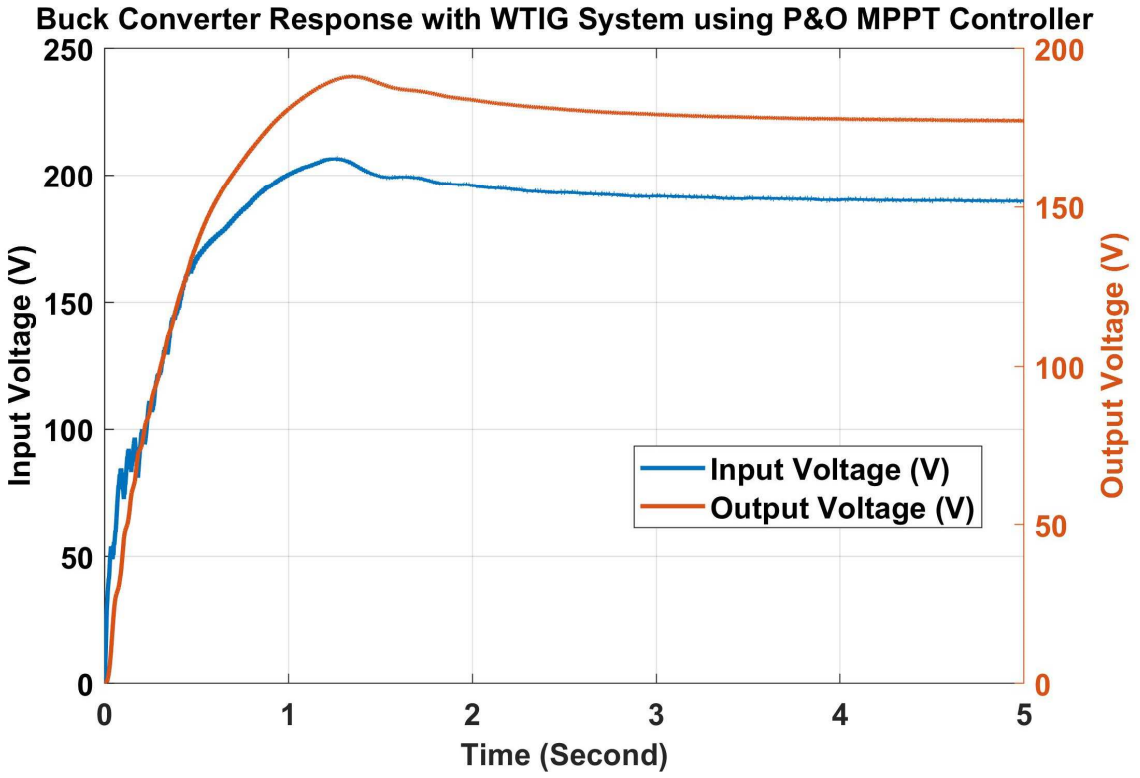

Figure 8. Input and Output Voltage of Buck Converter with WTIG System and P-&-O MPPT Controller.

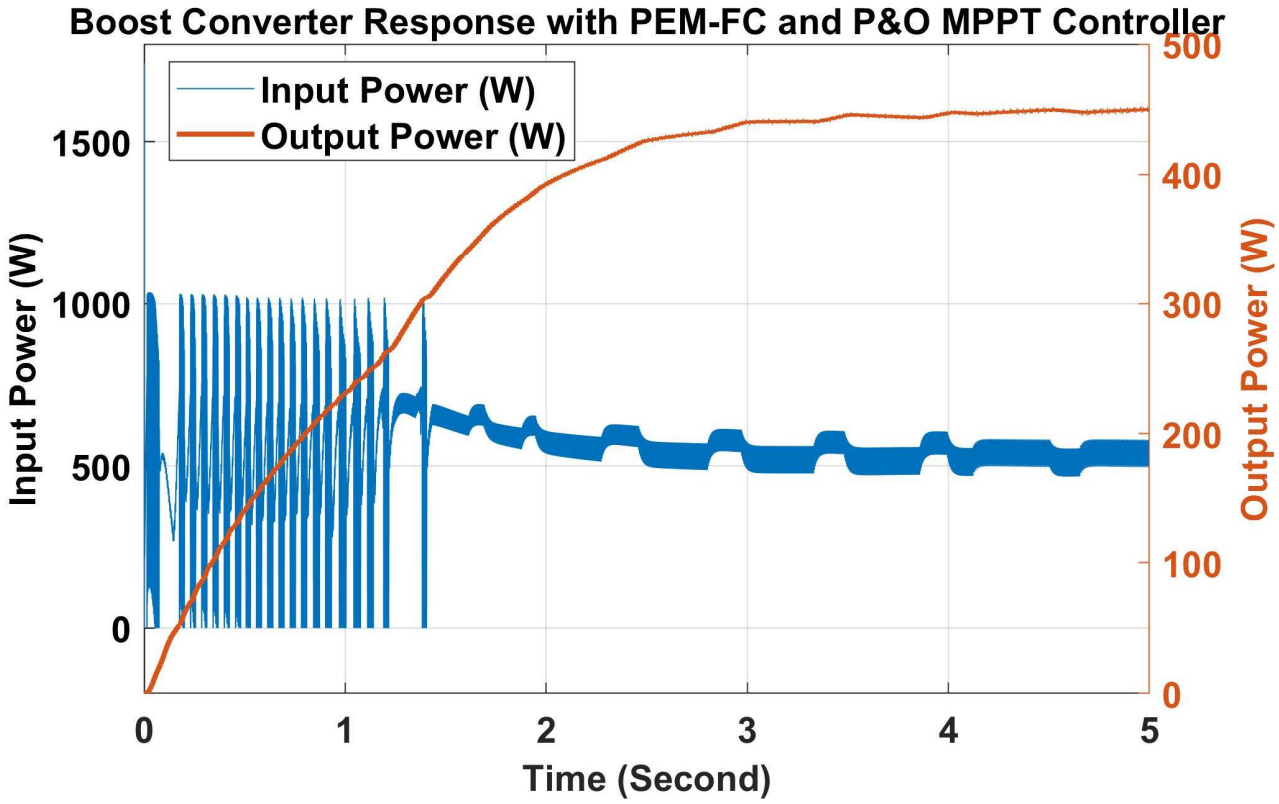

Figure 9. Input and Output Power of Boost Converter with PEM-FC and P-&-O MPPT Controller.

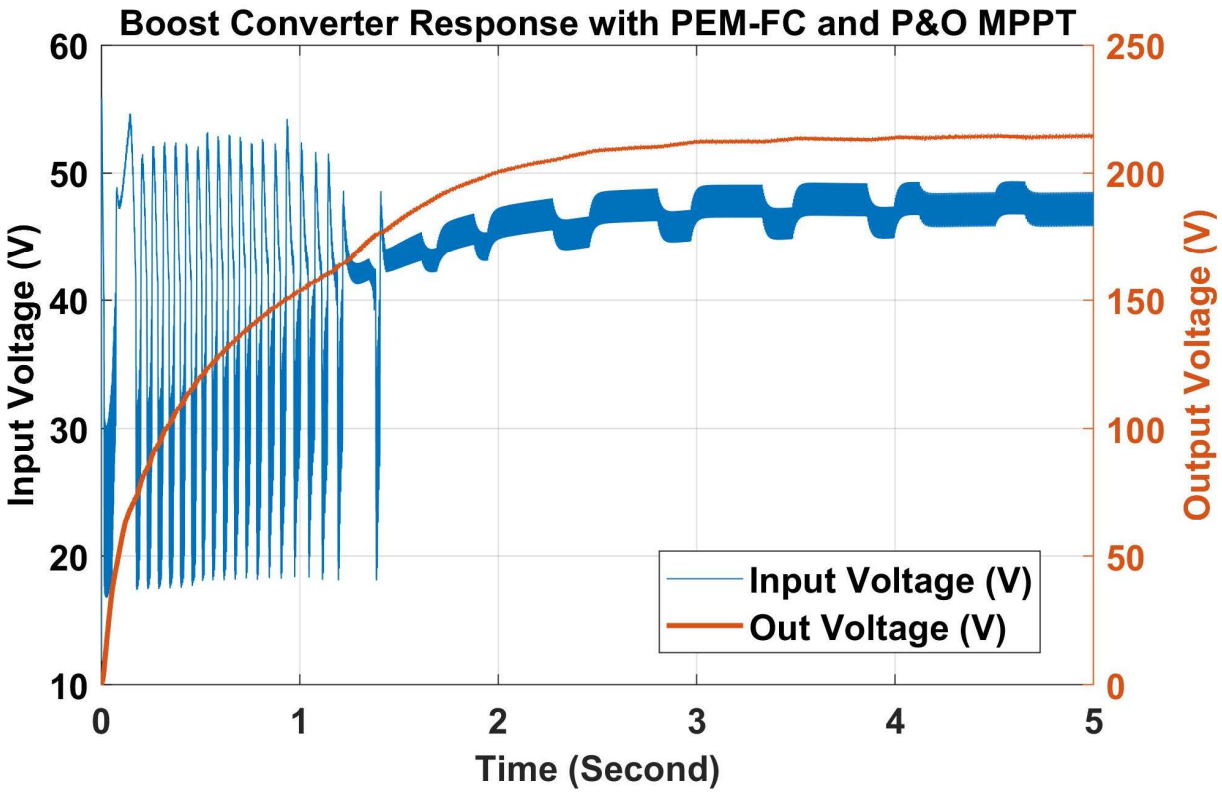

Figure 10. Input and Output Voltage of Boost Converter with PEM-FC and P-&-O MPPT.

The response of output power and voltage of hybrid RES using P-&-O controller and variation in SR, WS, and HFR for the value of 0.001 as duty-ratio perturbation are shown in Figure 11. Output power and voltage values of the proposed hybrid RES are recorded as 950 W and 175 V, respectively. The values of output power and voltage of the solar PV framework in favor of the boost converter, as shown in Figures 5 and 6, are 190 W, 270 W, 85 V and 190 V, respectively, using P-&-O MPPT controller. Similarly, for the WTIG system, as shown in Figures 7 and 8, the values of input and output power and voltage for the buck converter are 270 W, 320 W, 190 V, 150 V, respectively, with the P-&-O controller. The reduction in voltage is due to the buck converter. Figures 9 and 10 show the output power and voltage of the PEM-FC framework for the boost converter, as 415 W, 450 W, 45 V, and 180 V, respectively. The proposed hybrid RES using a P-&-O controller produces a higher output power of 950 W and output voltage of 175 V. A total simulation time of 5 s was used.

As per the simulation results, power production in steady-state conditions for the proposed hybrid RES is increased by 375%, 197% and 111%, more than the individual PV, WTIG and PEM-FC systems, respectively.

The investigator has performed the simulation by varying the ΔD, for the PV framework using the P-&-O technique and the results are shown in Figure 12 and Table 6. P&O MPPT with $\Delta D = 0.1$ shows a faster start-up response, while MPPT with $\Delta D = 0.01$ offers moderate, and MPPT with $\Delta D = 0.001$ shows a slower start-up response (or transient response). Steady-state oscillations have been observed to be higher in the case of $\Delta D = 0.1$, and moderate in the case of $\Delta D = 0.01$.

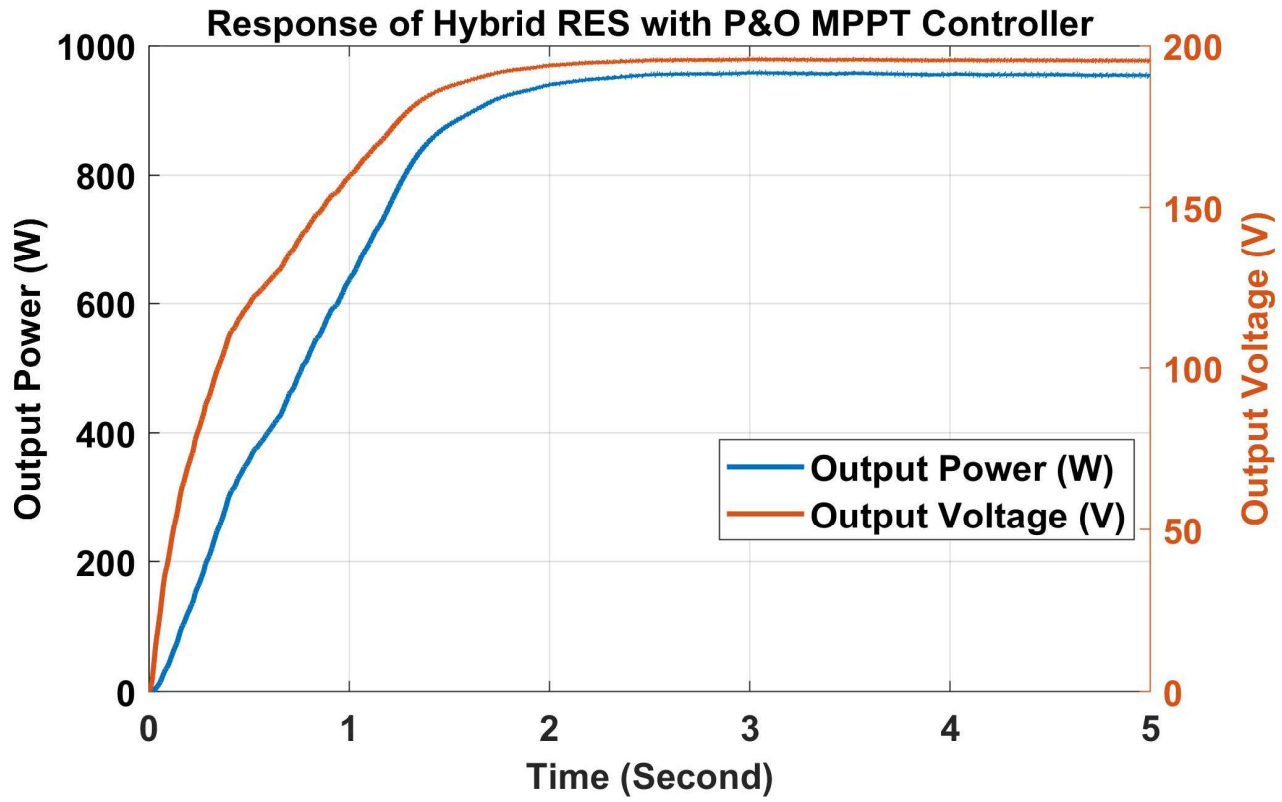

Figure 11. Output Power and Voltage of Hybrid RES with P-&-O MPPT.

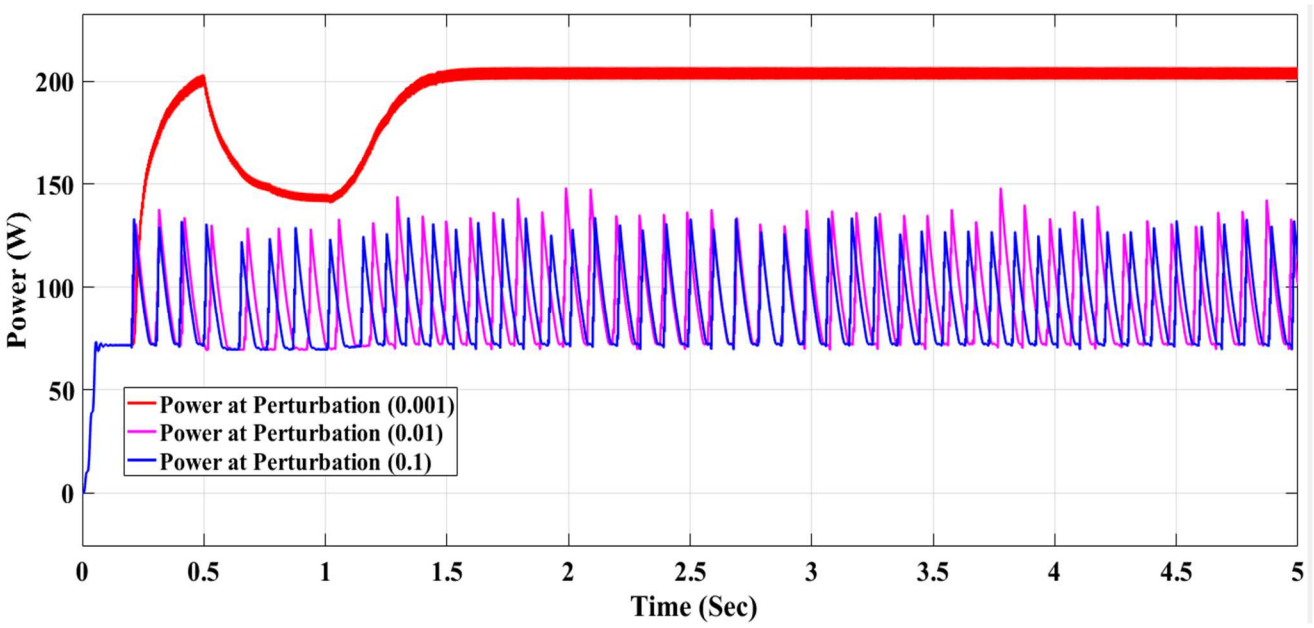

Figure 12. Power Analysis at ΔD = 0.001, ΔD = 0.01 and ΔD = 0.1 for PV System.

Table 6. Power Analysis at variable ΔD for PV System.

ΔD	Overshoot (%)	Transitions		Signal Statistics	
		Rise Time	Slew Rate	Amplitude	Time (s)
0.1	1.872	37.408 ms	1.522 (/ms)	134.3	3.263
0.01	191.067	333.056 µs	8.839 (/ms)	148.4	1.99
0.001	1.822	167.375 ms	642.381 (/s)	206.8	2.674

Good tracking performance has been found with $\Delta D = 0.001$ for a steady rise (ramp vary) in the radiation. It can be shown from the simulation results that the appropriate selection of ΔD can lead to maximum efficiency. In other words, the size of ΔD should not be extremely small or extremely enormous. It should be adopted with diligence.

3. F-LC MPPT Controller

In recent years, F-LC MPPT controllers based on artificial intelligence approaches have grown more popular than traditional systems due to their superior response, lack of overshoot and due to them having fewer oscillations in quick temperature, SR, and WS variations. The F-LC MPPT does not require a precise PV model for its design. The majority of the literature suggests using an F-LC MPPT with two inputs and one output. Error $E(k)$ and error change $\Delta E(k)$ are the two input variables [22].

$$E(k) = \frac{dI}{dV} + \frac{I}{V} \tag{5}$$

$$\Delta E(k) = E(k) - E(k-1) \tag{6}$$

where I is the RES's output current, dI is the change in current for two following instants specified by $[dI = I(k) - I(k-1)]$. V is the RES's output voltage, and dV is the change in voltage for the two following instants specified by $[dV = V(k) - V(k-1)]$.

One of the various approaches available for fuzzy inference can be used. The F-LC controller Mamdani's approach was largely employed, and the output $\Delta D(k)$ was computed using the center of gravity defuzzification method. Figure 13 shows the scheme of such an MPPT approach.

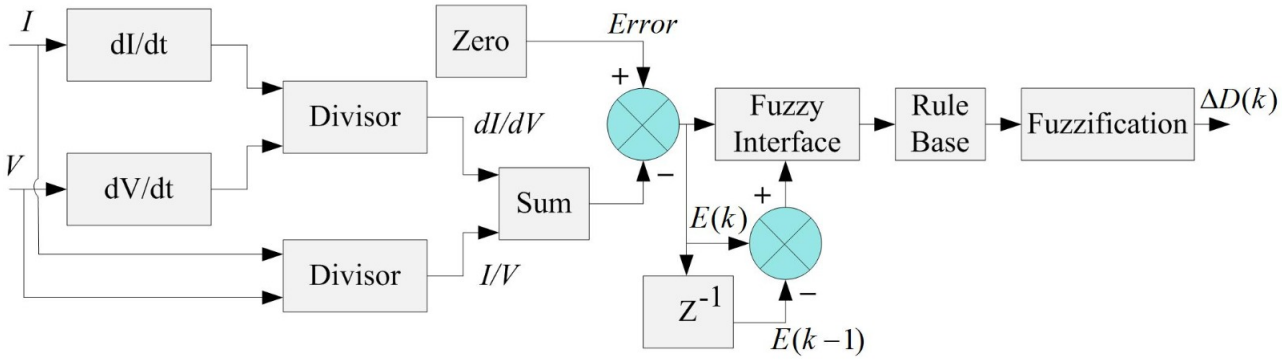

Figure 13. Block Diagram of F-LC MPPT.

Simulation Modelling of PV, WTIG, PEM-FC and Hybrid RES System with F-LC MPPT

The F-LC MPPT method was created and simulated in the MATLAB environment for a PV framework with a boost converter and resistive load. In the F-LC MPPT, the major control variables are identified and the sets that describe the significances of every linguistic variable and their range can be determined. $E(k)$ and $\Delta E(k)$ are the input variables. The linguistic variables are calculated from the input signals. The ΔD is the F-LC's system output. In Figure 14, the F-LC MPPT sub-system has been developed using $E(k)$, $\Delta E(k)$, and $\Delta D(k)$ variables.

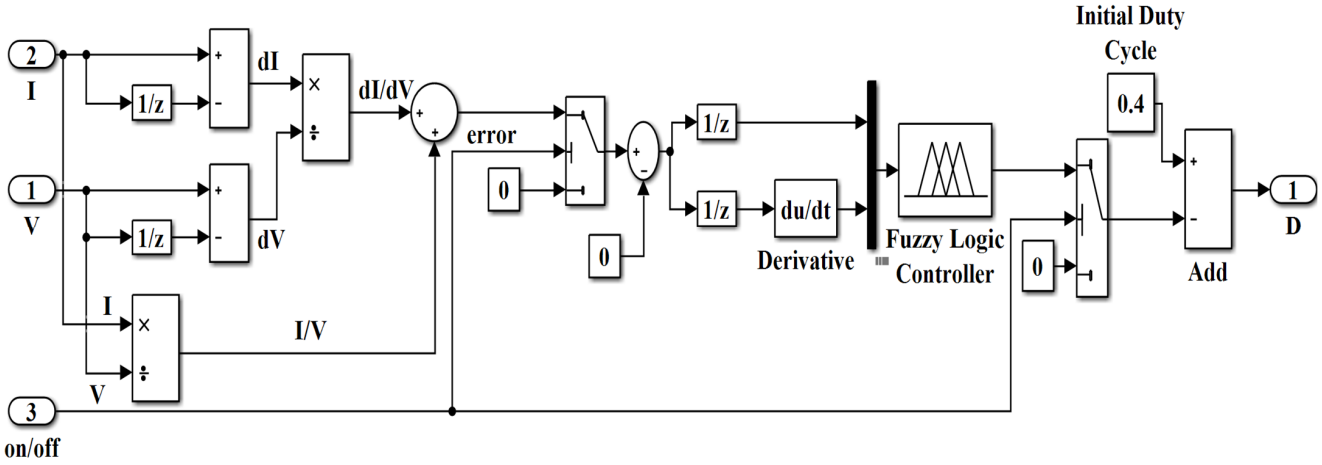

Figure 14. Sub-System for F-LC MPPT.

The triangular based membership functions are employed in the intuitive technique to fuzzify crisp value into membership value. The triangular based membership function fuzzifies variables like $E(k)$ and $\Delta E(k)$ into membership value in the proposed F-LC MPPT. The interval $(-5.0, 5.0)$ employed for PV system input variables are $E(k)$ and $\Delta E(k)$, as well as the interval $(-0.2, 0.2)$ for output variable $\Delta D(k)$.

There is only one dominating fuzzy subset for the proposed triangle type membership function that is recognized for any specific input. For membership functions, seven fuzzy sets are explored, which are defined in terms of linguistic variables such as negative-big (NB), negative-medium (NM), negative-small (NS), zero (ZE), positive-small (PS), positive-medium (PM), and positive-big (PB).

For input and output variables, seven triangle membership functions have been assigned. The F-LC MPPT was implemented using Mamdani's fuzzification approach and the centroid method of defuzzification. In Figure 15, the membership functions of the input and output variables are analyzed. Table 7 shows forth the rule framework.

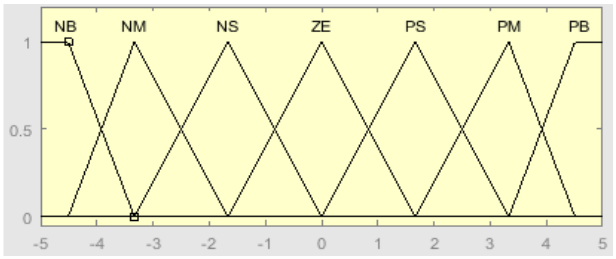

(**a**)

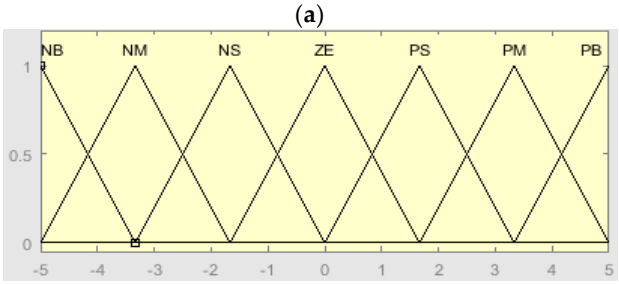

(**b**)

Figure 15. *Cont.*

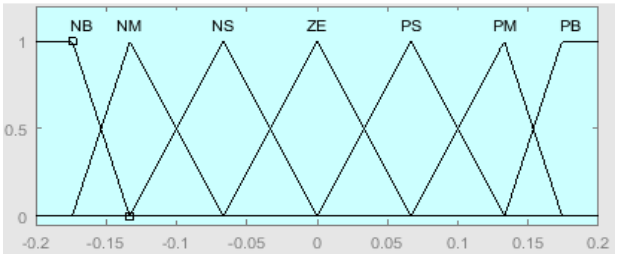

(**c**)

Figure 15. Input (**a**,**b**) and Output (**c**) Membership Functions of F-LC for PV System.

Table 7. Rule Base of F-LC for PV System.

$\Delta D(k)$		$E(k)$						
		NB	**NM**	**NS**	**ZE**	**PS**	**PM**	**PB**
$\Delta E(k)$	**NB**	ZE	ZE	NM	NS	PM	PM	PB
	NM	ZE	ZE	NS	ZE	PM	PS	PB
	NS	ZE	ZE	ZE	ZE	PM	PS	PB
	ZE	NM	NB	ZE	NM	PM	PS	PB
	PS	NM	BB	ZE	NM	ZE	ZE	ZE
	PM	NM	NB	PS	NM	ZE	ZE	ZE
	PB	NM	NB	PM	NM	ZE	PS	ZE

In the MATLAB/SIMULINK platform, F-LC MPPT was created and simulated for a WTIG with a buck converter and resistive load.

For input and output variables, five triangle membership functions have been assigned. The F-LC MPPT was implemented using Mamdani's fuzzification approach and the centroid method of defuzzification. Figure 16 shows the membership functions of input and output variables. For the WTIG system, the interval ranges for variables such as $E(k)$, $\Delta E(k)$ and $\Delta D(k)$ are $(-6, 6)$, $(-250, 250)$ and $(-0.2, 0.2)$, respectively. The rule base is given in Table 8.

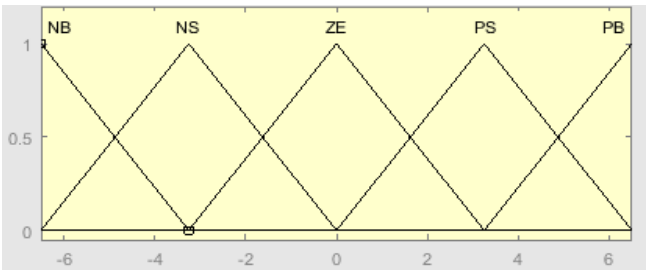

(**a**)

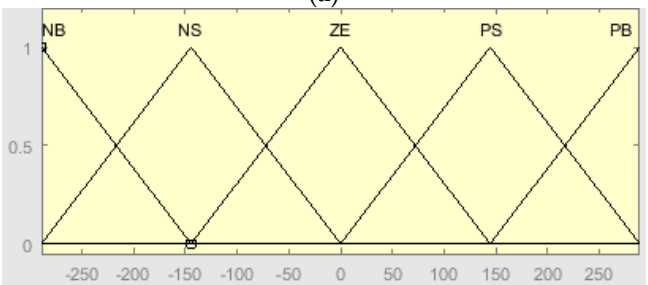

(**b**)

Figure 16. *Cont.*

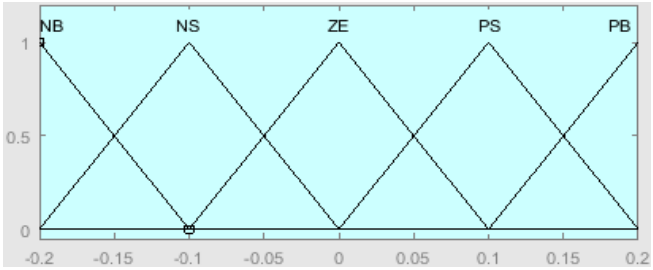

(**c**)

Figure 16. Input (**a**,**b**) and Output (**c**) Membership Functions of F-LC for WTIG System.

Table 8. F-LC MPPT for WTIG System Rule Base.

$\Delta D(k)$		$E(k)$				
		NB	**NS**	**ZE**	**PS**	**PB**
$\Delta E(k)$	**NB**	ZE	NS	ZE	NM	PM
	NS	ZE	ZE	ZE	NS	PS
	ZE	ZE	ZE	ZE	ZE	PS
	PS	NM	NM	NB	ZE	PS
	PB	NM	NM	BB	ZE	ZE

In the MATLAB/SIMULINK platform, F-LC MPPT was built and simulated for PEM-FC with a boost converter and resistive load. The triangle type membership functions of input and output variables are given in Figure 17 for the PEM-FC system. For the PEM-FC system, the interval range of membership functions for the variables such as $E(k)$, $\Delta E(k)$ and $\Delta D(k)$ are (10, 12), (46.5, 49) and (−0.2, 0.2), respectively. Table 9 shows the rule framework.

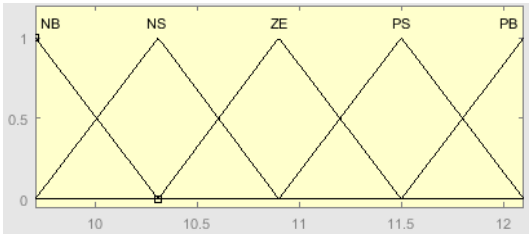

(**a**)

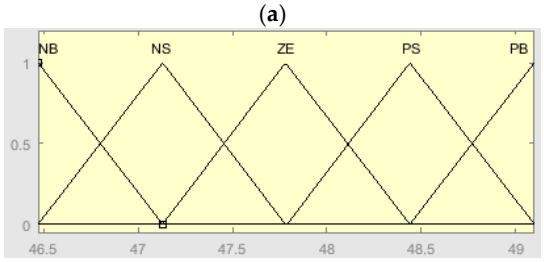

(**b**)

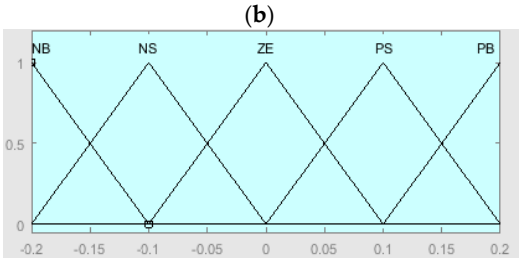

(**c**)

Figure 17. Input (**a**,**b**) and output (**c**) Membership Functions of F-LC for PEM-FC System.

Table 9. Rule Base for F-LC MPPT for PEM-FC System.

$\Delta E(k)$		$E(k)$				
		NB	**NS**	**ZE**	**PS**	**PB**
$\Delta D(k)$	**NB**	NB	NS	NS	ZE	ZE
	NS	NB	NS	NS	ZE	PS
	ZE	NS	NS	ZE	PS	PS
	PS	NS	ZE	PS	PS	PB
	PB	ZE	ZE	PS	PS	PB

The hybrid RES using F-LC MPPT and load has been created and simulated in the MATLAB/SIMULINK platform. Tables 1, 3 and 5 show the simulation parameters that were used in the Matlab/Simulink model. The input variation test patterns are used and presented in Figures 2–4. The output power and voltage of PV, WTIG, PEM-FC and hybrid RES with F-LC MPPT have been obtained.

The output power and voltage of the PV framework using a boost converter and F-LC MPPT, as a function of SR intensity, are shown in Figure 18. The output voltage is 150 V, with the output power being 230 W. When compared to the P-&-O controller's output power response, Figure 18 demonstrates a reduction in fluctuations, indicating that F-LC MPPT delivers greater performance. Figure 19 shows the output power and voltage of the WTIG system using a buck converter and with F-LC against the variation in WS as per the test pattern shown in Figure 3. In this regard, the stable value of output power and output voltage are 340 W and 175 V. The PEM-FC system also behaved similarly with the test pattern, as shown in Figure 4, and provided power and voltage values of 460 W and 210 V, as shown in Figure 20. The hybrid RES produced power and voltage values of dc-link as 1000 W, 175 V, as shown in Figure 21.

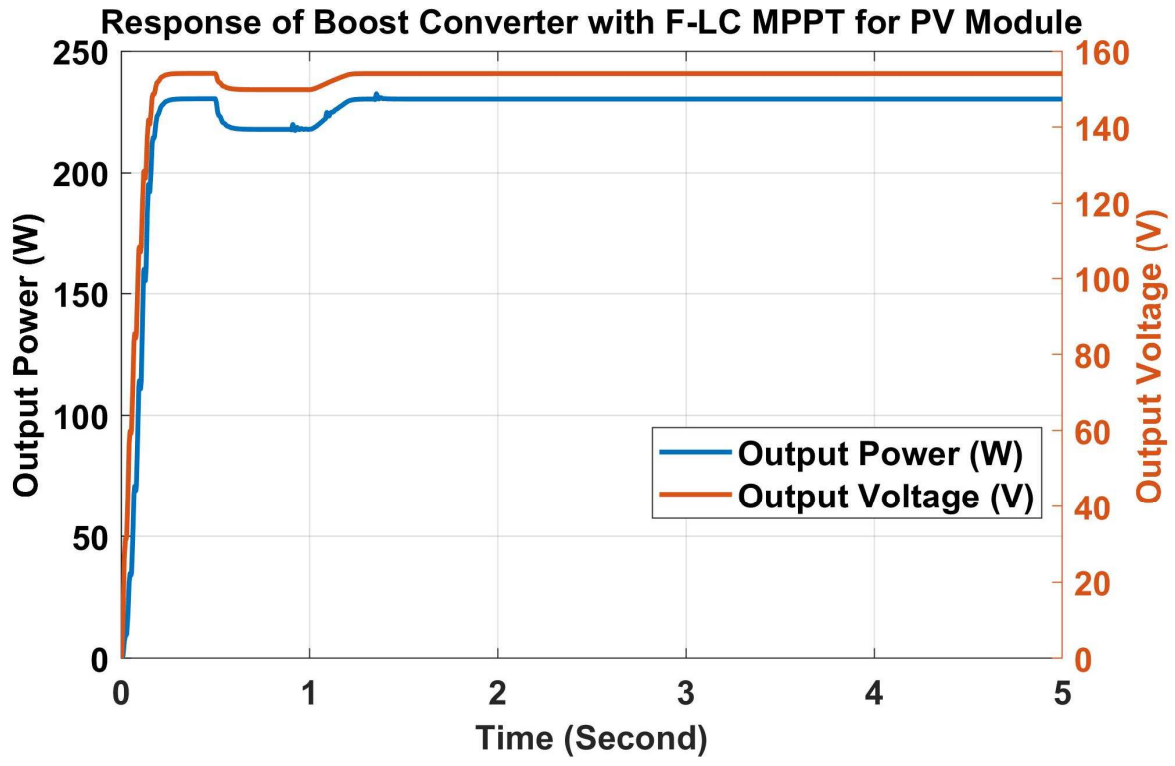

Figure 18. Output Power and Voltage of Boost Converter with F-LC MPPT for PV Module.

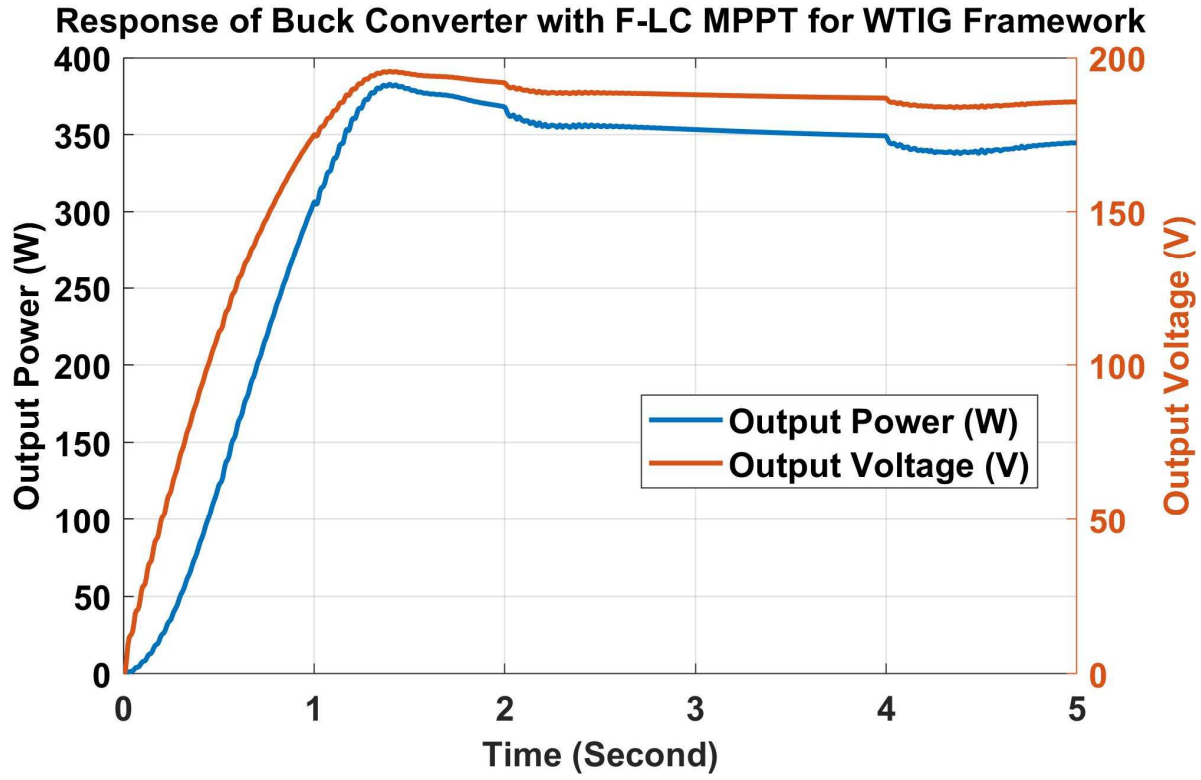

Figure 19. Output Power and Voltage of Power Buck Converter with F-LC MPPT for WTIG Framework.

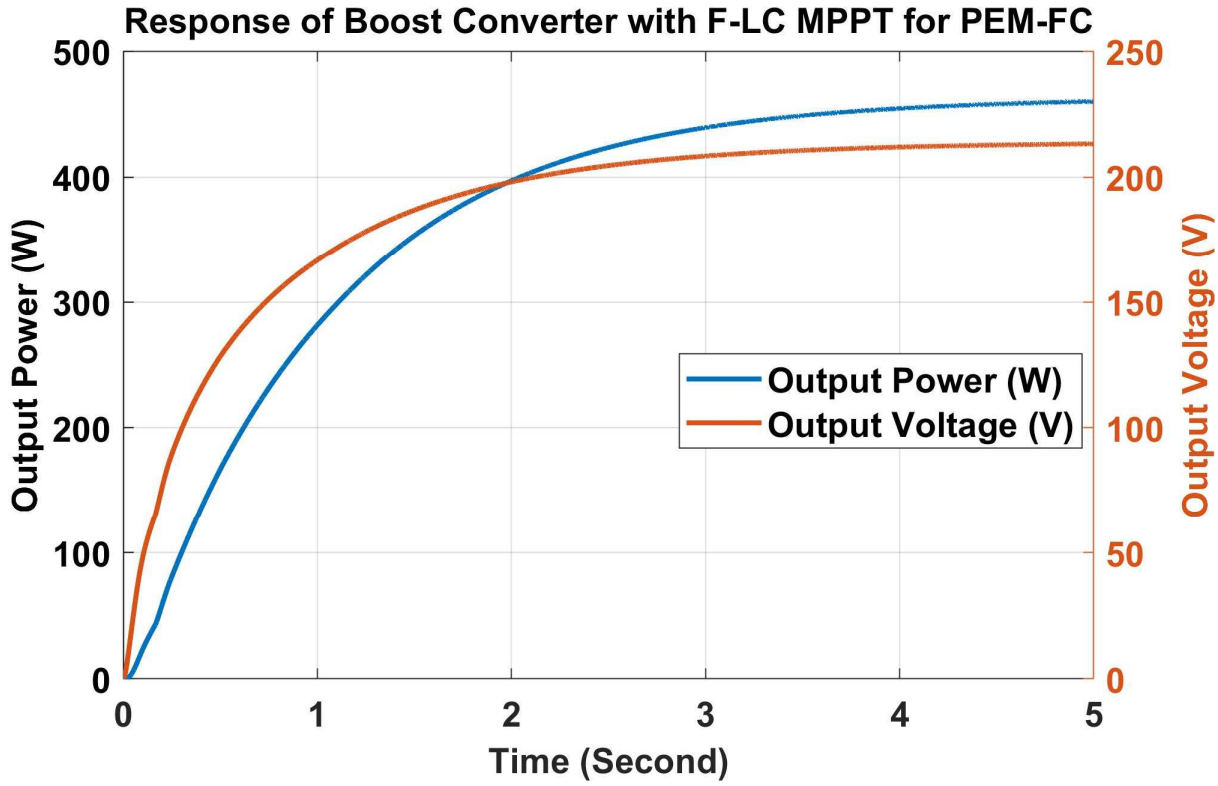

Figure 20. Output Power and Voltage of Boost Converter with F-LC MPPT for PEM-FC Framework.

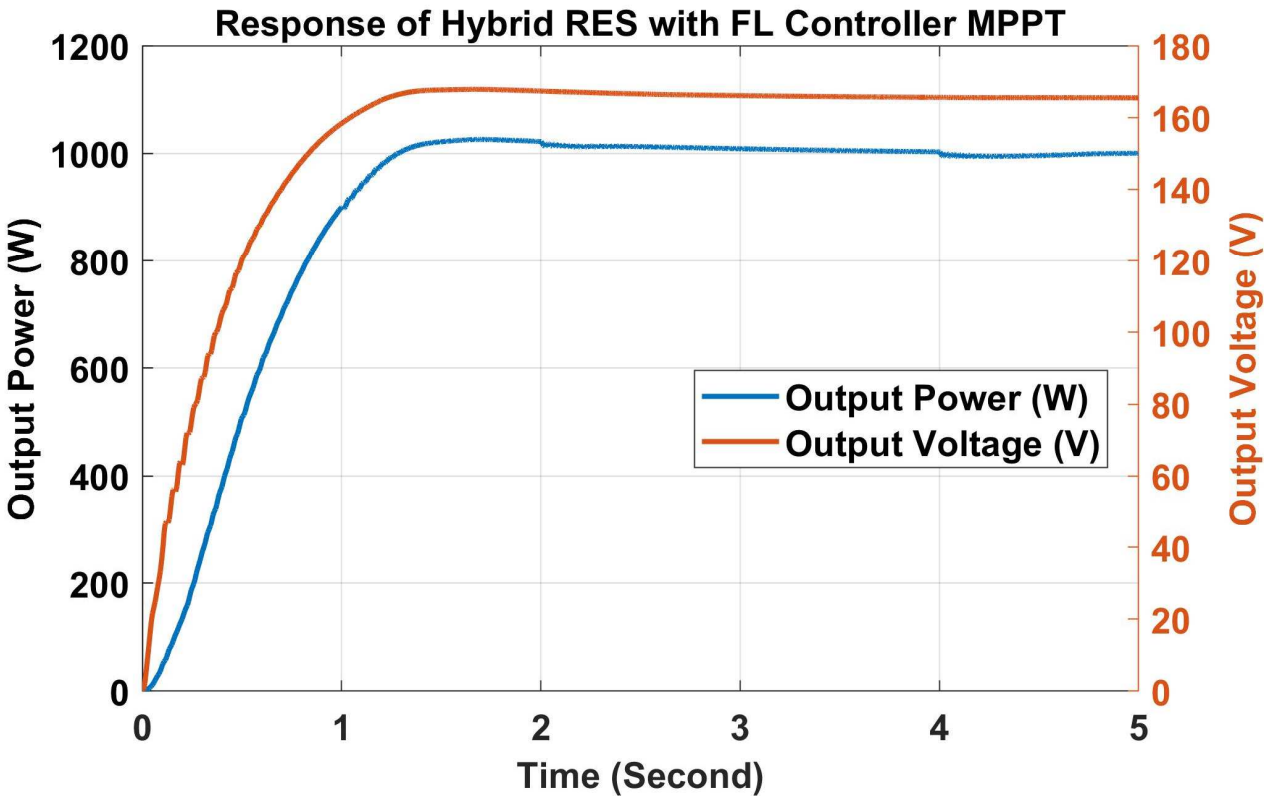

Figure 21. Output Power and Voltage of Hybrid RES with F-LC MPPT.

A comparative study of the output-power characteristics of Figures 7 and 19 for the WTIG system, with Figures 9 and 20 for the PEM-FC system, show that the steady-state fluctuations have been significantly abridged with the F-LC technique as compared to the conventional P-&-O MPPT controller. No overshoot has been observed in any of these output responses. Better tracking, without oscillations of the input variation, i.e., a step-change in SR and WS, and a ramp change in HFR has been observed.

The output responses of the hybrid RES, as shown in Figure 21, is an improved version of that given in Figure 11. Hence, it can be clearly stated that F-LC MPPT gives better results than the P-&-O MPPT controller. PV, WTIG, PEM-FC, and hybrid RES produced 230 W, 340 W, 460 W, and 1000 W of electricity in steady-state conditions, correspondingly. It is understandable that the power generation of the hybrid RES is higher than the PV system by 335% $\left(\frac{(1000-230)}{230} \times 100\right)$ and 194% $\left(\frac{(1000-340)}{340} \times 100\right)$ more than the WTIG system and 117% $\left(\frac{(1000-460)}{460} \times 100\right)$ more than the PEM-FC system. Therefore, the hybrid RES is found to be a better option.

4. Scheme of AN-N MPPT Controller

For non-linear and complicated systems, the AN-N MPPT offers the best answer. In this regard, the backpropagation based AN-N MPPT is used in this proposed model. AN-N MPPT model is a black box that does not necessitate comprehensive information about the non-linear framework [23–27].

To track MPP, two-layer feedforward AN-N architecture was used in this study to generate duty-ratio. The external data is received in the form of voltage and current in the input region. The hidden neurons in the first layer (hidden layer) obtain data from the input region, and deliver it to the second layer, i.e., output layer. This technique is shown in Figure 22.

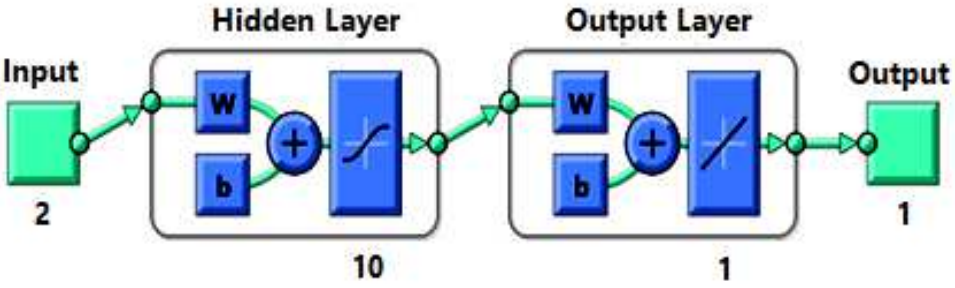

Figure 22. AN-N Model.

The voltage input layer is now being recorded from a real-time framework in various SR, temperature, WS, and HFR cases. The hidden layer consists of ten nodes. Equation (2) provides the relationship between inputs and outputs [28,29]:

$$n_j^1 = \sum_{i=1}^{2} w_{ji} x_i + b_j^1,\ j = 1 \sim 10 \tag{7}$$

where w_{ji} represents the weighting given to the ith input unit's link, and b_j^1 is the bias of the hidden layer neurons. The hidden layer's neurons provide the Equation (8):

$$a_j^1 = f_1\left(\sum_{i=2}^{2} w_{ji} x_i\right), f_1(x) = purelin(x) = x \tag{8}$$

The net input to the neurons during the output layer can be expressed by Equation (9):

$$n_k^2 = \sum_{i=1}^{1} w_{kj} a_j^1 + b_k^2,\ k = 1 \sim 4 \tag{9}$$

where w_{kj} is the weight on the jth input unit's connections, and b_k^2 is the bias for the second layer neurons. The network output of interest is a, a_k^2 from the second layer, and these outputs are denoted as y_k and given by Equation (10):

$$a_k^2 = y_k = f_2\left(\sum_{j=1}^{10} w_{kj} + b_k^1\right), f_2(x) = purelin(x) = x \tag{10}$$

Function fitting is the process of training an AN-N on a set of inputs to produce an associated set of target outputs. The AN-N develops a generalization of the input–output connection after fitting the data, which it can use to generate outputs for inputs it has not been trained on. Training data is sent into the network during training, and the network is altered based on its inaccuracy. Validation data has been used to assess network generalization, and to end training when generalization has reached a plateau. Testing data provide an unbiased assessment of network performance before and after training.

Modelling and Analysis of AN-N MPPT

The voltage and current based on ecological data such as SR, WS, and HFR can be used as inputs for AN-N system. The "*D*" is used to drive the dc–dc power converter, for MPP is the output of the AN-N. To train the network, experimental measurements or model-based simulation results can be used as input data. The AN-N can track the MPP after training using the input data. A two-layer feed-forward AN-N with 10 sigmoid hidden neurons is created using the AN-N toolbox in MATLAB/SIMULINK. The network was trained with an experimental set of input data using the Levenberg–Marquardt backpropagation technique. A total of 1000, 5398, and 5000 samples were collected from the PV, WTIG, and

PEM-FC systems' real-time experimental settings, respectively. Out of these, samples such as 700, 3778, and 3500 are used for network training purposes, and the remaining samples were utilized for validation and testing.

AN-N has been used as a sub-system in the models of PV system with a boost converter, WTIG system with a buck converter and PEM-FC system with a boost converter. These systems are connected in parallel with dc-link. This creates the hybrid RES shown in Figure 23.

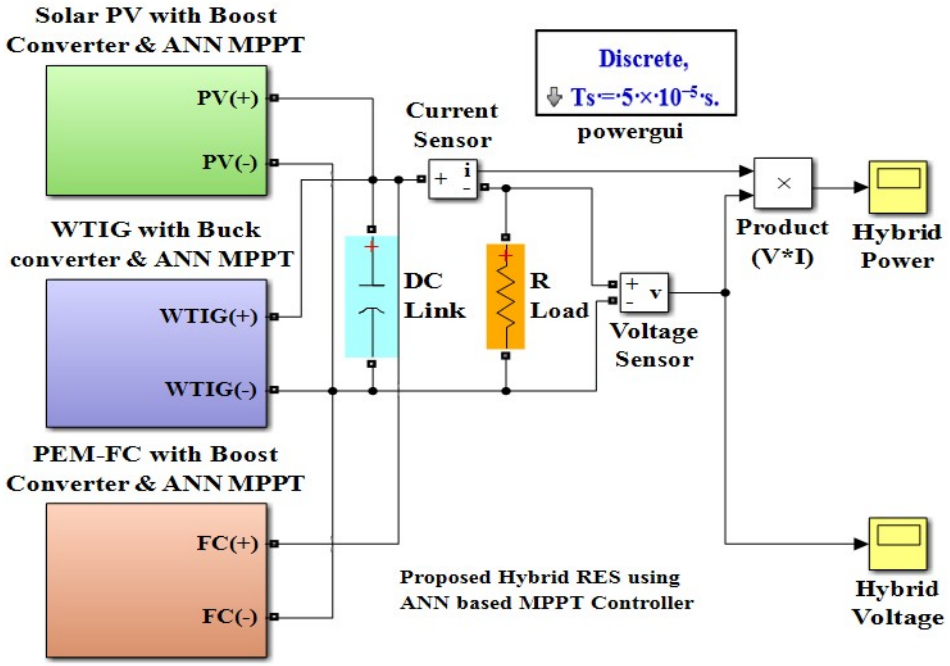

Figure 23. Modelling of Proposed Hybrid RES with AN-N MPPT.

The mean square error (MSE) and regression of the AN-N model are shown in Table 10. The MSE shows the link between the outputs and the targets, whereas regression reveals the average squared difference between the outputs and the targets. A close association is represented by a regression value of one, whereas a random relationship is represented by a regression value of "0".

Table 10. Process of MSE and Regression for Training, Validation and Testing.

Sr. No.	Procedure	No. of Samples	MSE	Regression
		For PV		
1	Training	700.0	1.047×10^{-5}	1.660×10^{-1}
2	Validating	150.0	1.239×10^{-5}	1.334×10^{-1}
3	Testing	150.0	1.015×10^{-5}	8.617×10^{-2}
		For WTIG		
1	Training	3778	8.23371×10^{-2}	2.486×10^{-1}
2	Validating	810	7.98225×10^{-2}	2.33441×10^{-1}
3	Testing	810	8.55248×10^{-2}	2.2827×10^{-1}
		For PEM-FC		
1	Training	3500	8.43061×10^{-2}	1.55297×10^{-1}
2	Validating	750	7.80607×10^{-2}	2.19705×10^{-1}
3	Testing	750	8.51936×10^{-2}	5.60816×10^{-1}

PV, WT, FC, and hybrid RES combined with AN-N MPPT were simulated and results were obtained. The simulation parameters and input variable test patterns are identical. The responses of the power and voltage of PV, WTIG, and PEM-FC systems output for dc–dc converters are studied. Figures 24–27 demonstrate the responses of output power and voltage to changes in SR, WS, and HFR, as well as a load with AN-N MPPT, for PV, WTIG, PEM-FC, and hybrid RES. These output responses are similar to those produced when F-LC MPPT is linked, as shown in Figures 18–21.

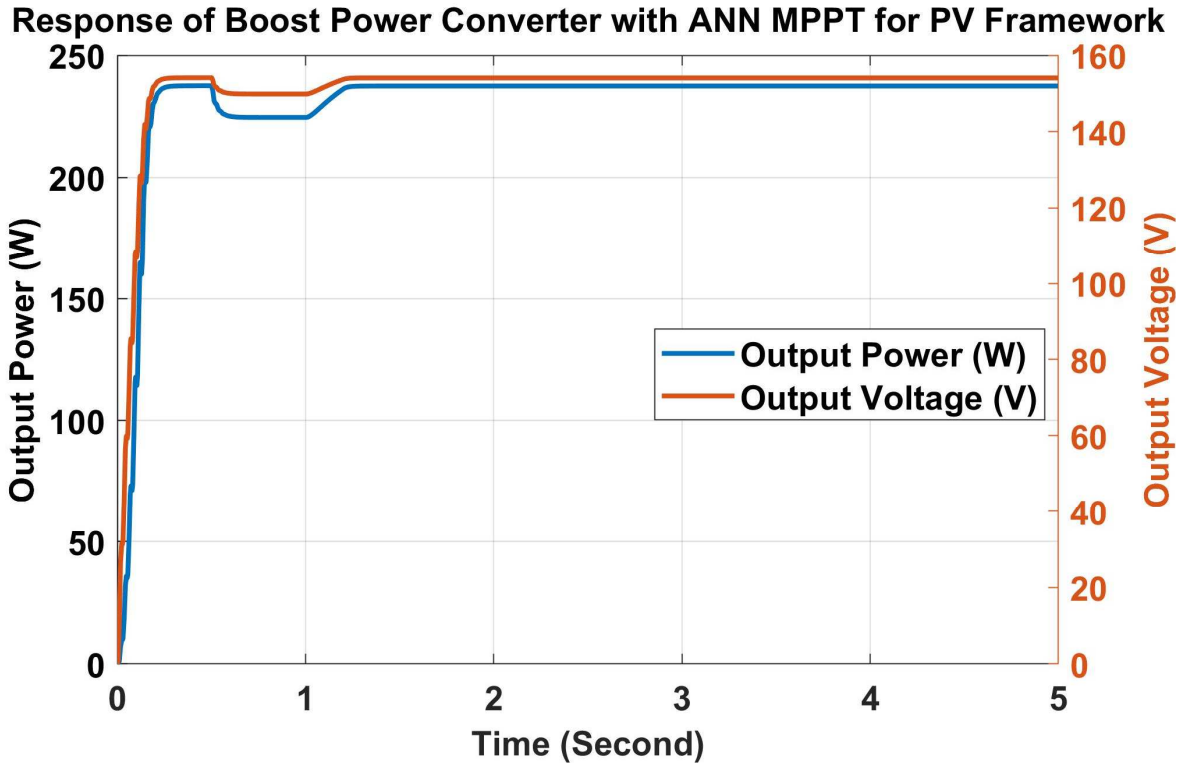

Figure 24. Output Power and Voltage of Boost Power Converter with AN-N MPPT for PV Framework.

The characteristics of output power and voltage of the various systems in the discussion were compared by using the P-&-O technique, F-LC, and AN-N MPPT. There was no overshoot and no oscillations in the tracking. It is concluded that the AN-N MPPT controller operates similarly to the F-LC MPPT controller, but outperforms the P-&-O MPPT controller. The PV framework with a boost converter using AN-N MPPT produces steady output power and voltage significances of 240 W and 155 V, respectively. Figure 25, the values of stable output power and voltage of WTIG system using a buck converter and AN-N MPPT are found to be 350 W and 175 V, respectively. The PEM-FC system also behaves similarly, and provided output power and voltage significances as 465 W and 210 V, as shown in Figure 26. The hybrid RES produced power and voltage values of dc-link as 1040 W, 175 V, as shown in 27. In this case, moreover, the power production of hybrid RES is higher than the PV system by 333%, 197% higher than the WTIG system, and 124% higher than the PEM-FC system. Thus, the hybrid RES is found to be a better option.

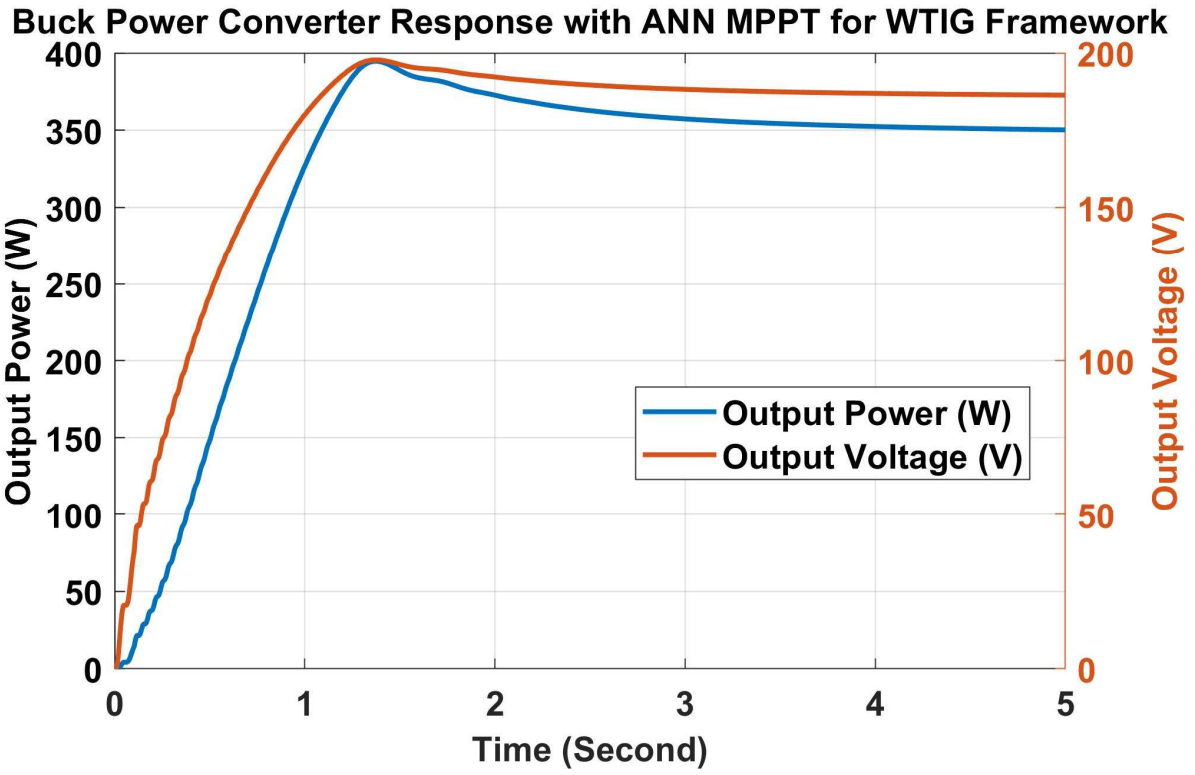

Figure 25. Output Power and Voltage of Buck Power Converter with AN-N Technique for WTIG Framework.

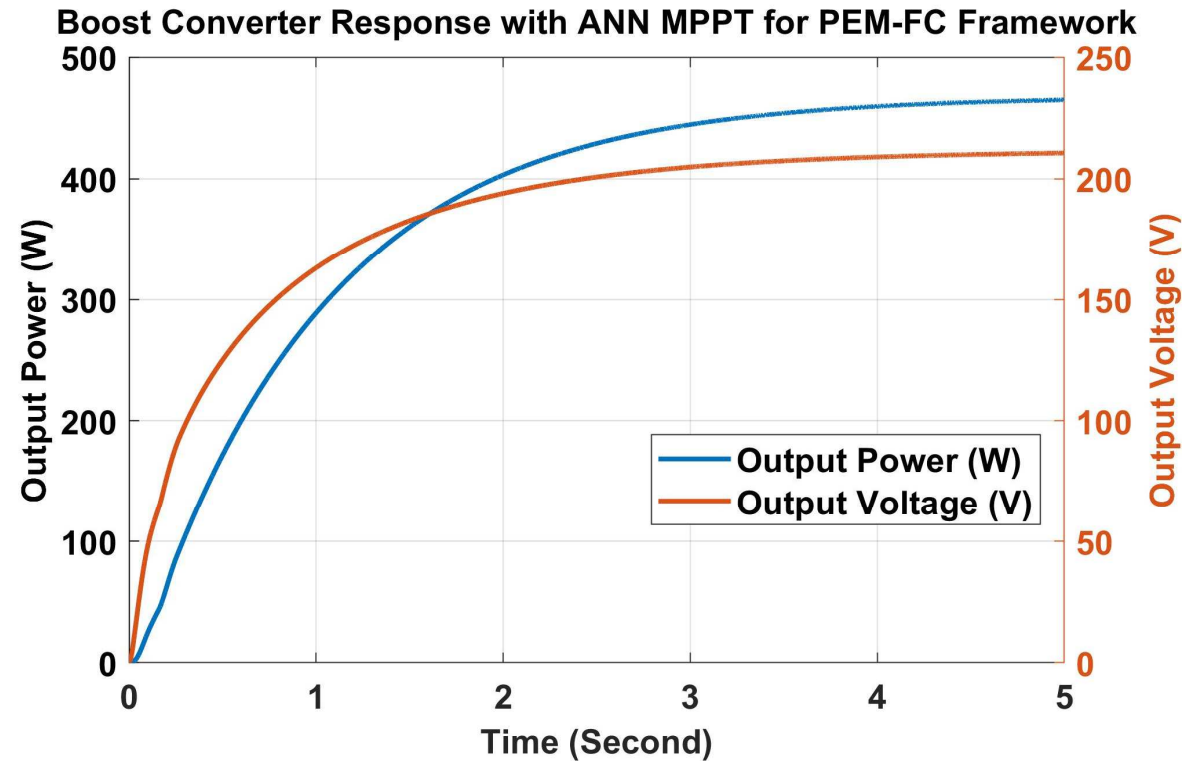

Figure 26. Output Power and Voltage of Boost Converter with AN-N Technique for PEM-FC Framework.

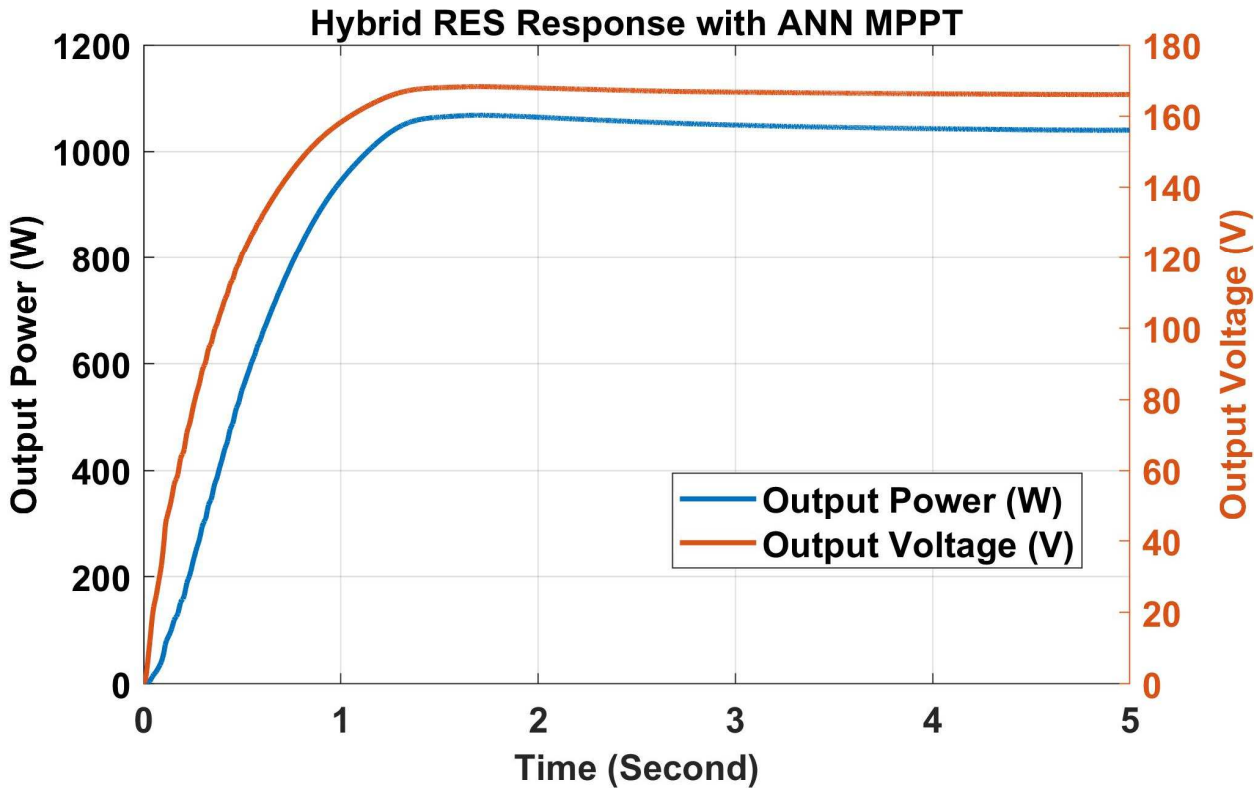

Figure 27. Output Power and Voltage of Hybrid RES with AN-N MPPT.

5. AN-FIS MPPT Controller

AN-N and F-LC are combined in AN-FIS. With fuzzy rules and membership functions, F-LC can convert linguistic concepts into numerical values. Finding accurate fuzzy rules, and membership functions that heavily rely on framework performance, on the other hand, can be difficult. Although the AN-N is a tool designed for mapping nonlinear functions, it is a black-box model. To alleviate the disadvantages of the separate approaches, AN-FIS combines AN-N and F-LC [30–33].

The AN-FIS MPPT system, when properly adjusted, can track MPP with greater precision than the P-&-O approach [34]. Figure 28 shows a typical AN-FIS based MPPT approach in RES. The AN-FIS algorithm takes voltage and current as inputs and generates a "*D*" to control the semiconductor switch in the dc-dc converter to follow the MPP.

The AN-FIS MPPT has six layers, as shown in Figure 28. The input layer is made up of neurons that send a strong input signal from the outside to layer 2. The second layer is the fuzzification layer, which contains neurons that perform the fuzzification process. The third layer is the rule-base layer. Each neuron in this layer corresponds to a fuzzy rule. A rule neuron calculates the rule's firing strength using input from the fuzzification neurons that it represents. The fourth layer is the normalization layer, which determines the normalized firing strength of each rule by taking input from all neurons in the rule-base layer. The defuzzification layer is made up of neurons that are connected to normalization neurons, and that receive input signals to calculate the weighted consequence value of a rule. A single summation neuron represents Layer 6, which adds together all of the defuzzification neurons' outputs to generate the total AN-FIS outputs.

The AN-FIS controller was designed in this study with two inputs such as voltage and current, and one output indicating the "*D*". The Sugeno inference model must be used to create the fuzzy rule-base designed for this MPPT controller. The AN-FIS model's structure is represented in Figure 29.

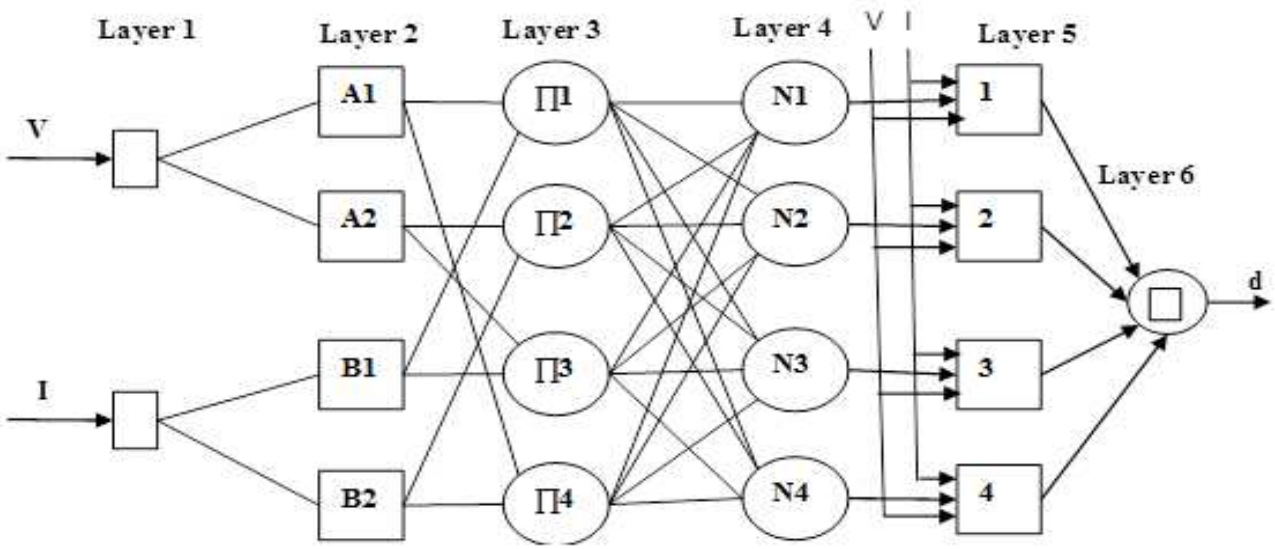

Figure 28. AN-FIS MPPT Scheme.

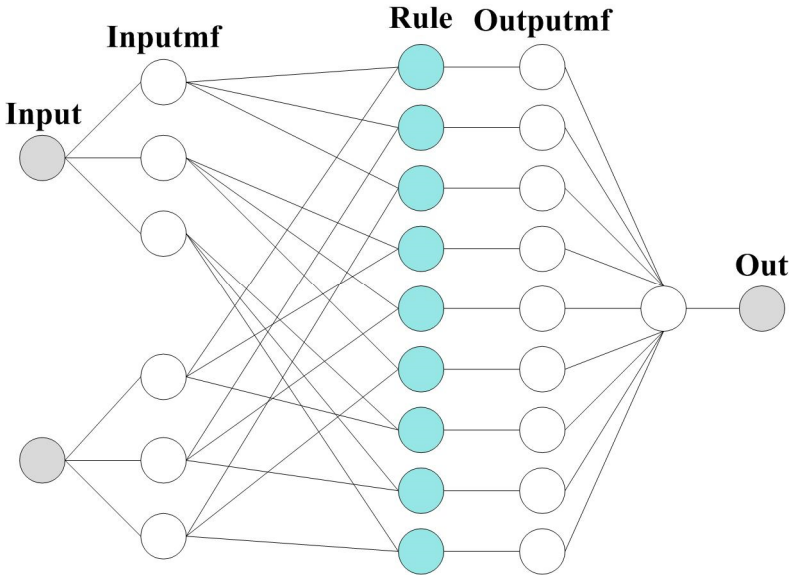

Figure 29. AN-FIS Model configuration.

The training data is identical to that used in the AN-N MPPT design. The AN-FIS controller was designed using the MATLAB anfisedit tool, and using two neurons in layer 1 and 14 neurons in the fuzzification layer. Modelling of the hybrid RES using AN-FIS MPPT, as shown in Figure 30, has been carried out.

The results were obtained after the development and simulated PV, WTIG, PEM-FC, and hybrid RES models with AN-FIS MPPT. The simulation parameters and input variation test patterns for PV, WTIG, PEM-FC, and hybrid RES are the same as those used in the other scenarios. The responses of output power and voltage by deviations in SR, WS, HFR, load and with AN-FIS technique for PV, WTIG, PEM-FC, and hybrid RES are shown in Figures 31–34.

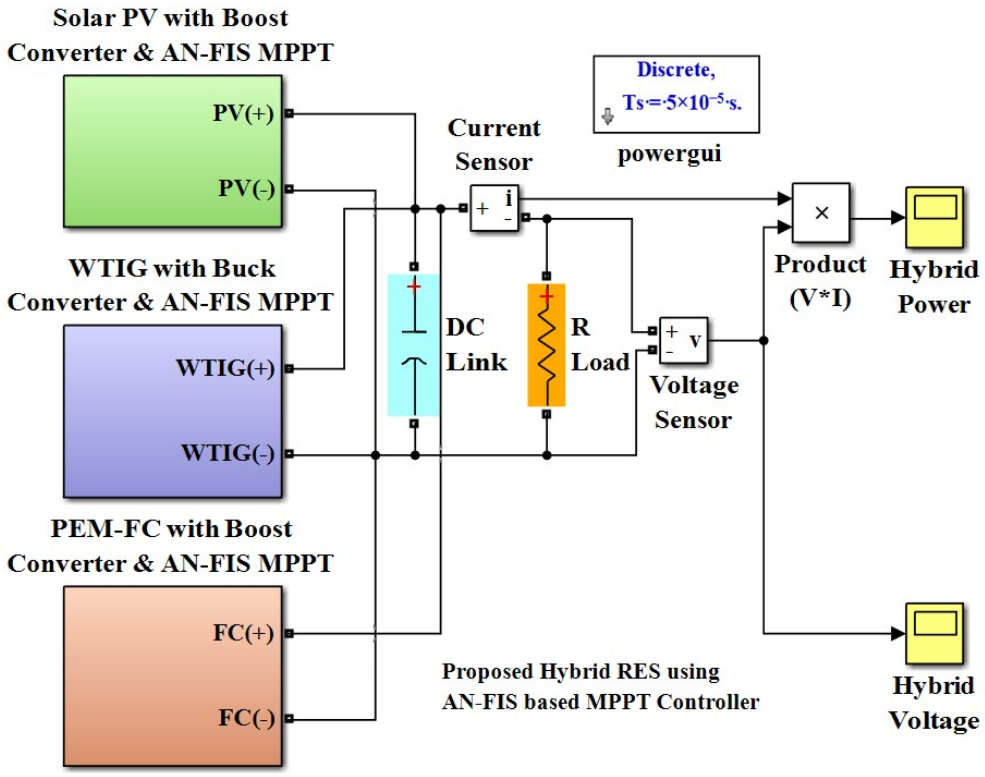

Figure 30. Modelling of Proposed Hybrid RES with AN-FIS MPPT.

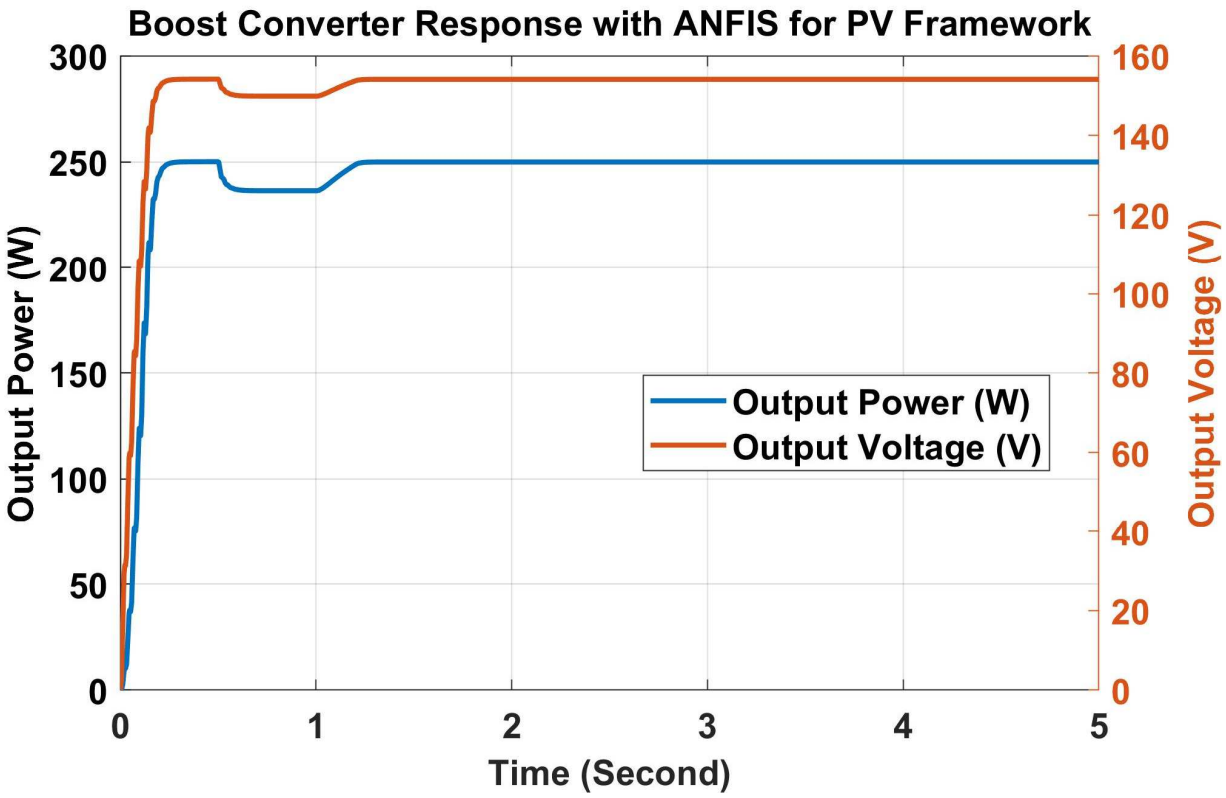

Figure 31. Output Power and Voltage of Boost Converter with AN-FIS MPPT for PV Framework.

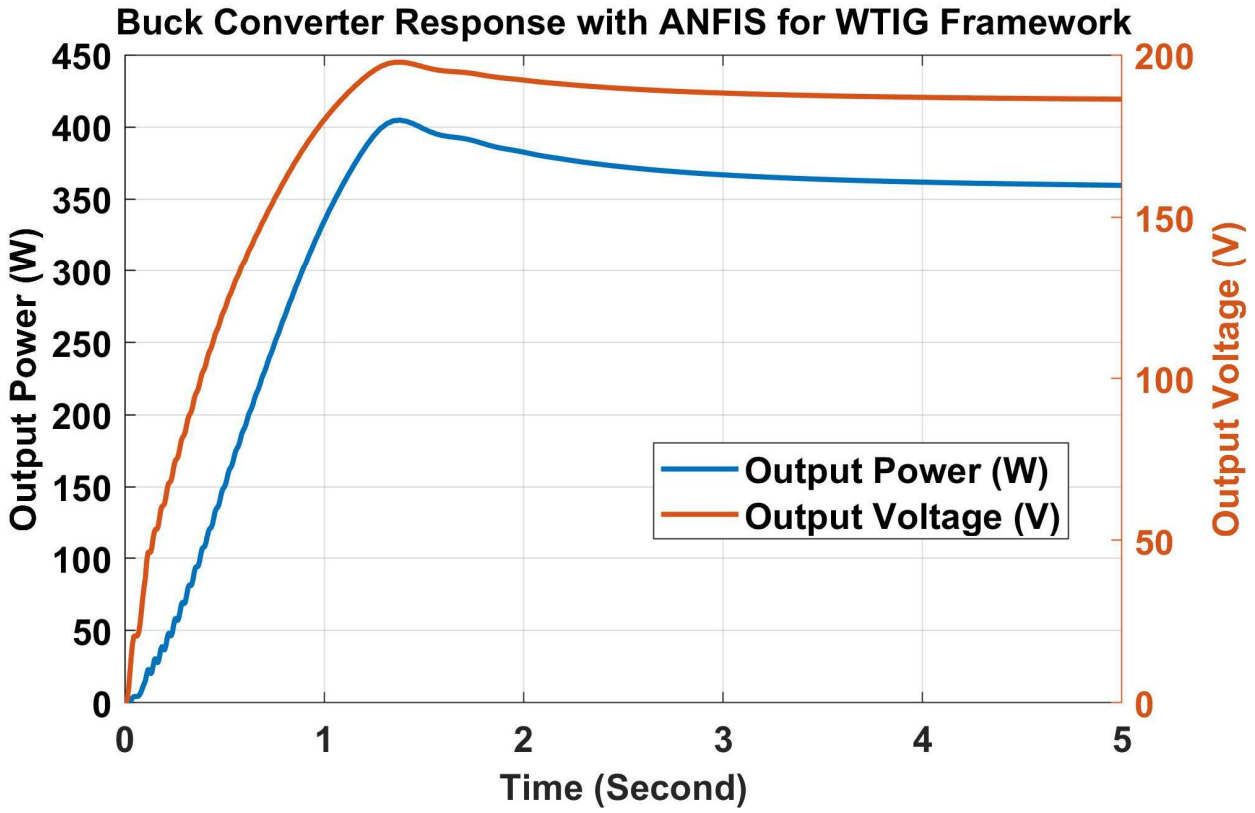

Figure 32. Output Power and Voltage of Buck Converter with AN-FIS MPPT for WTIG Framework.

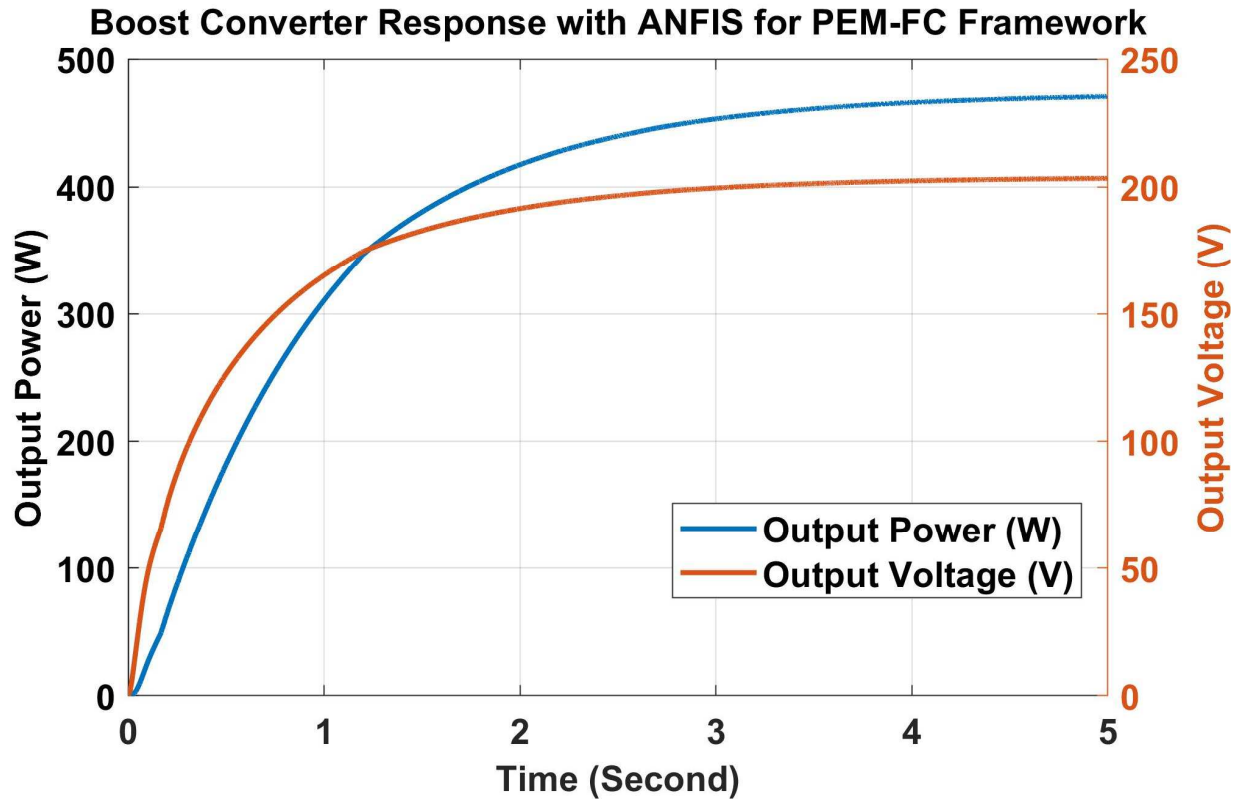

Figure 33. Output Power and Voltage of Boost Converter with AN-FIS MPPT for PEM-FC Framework.

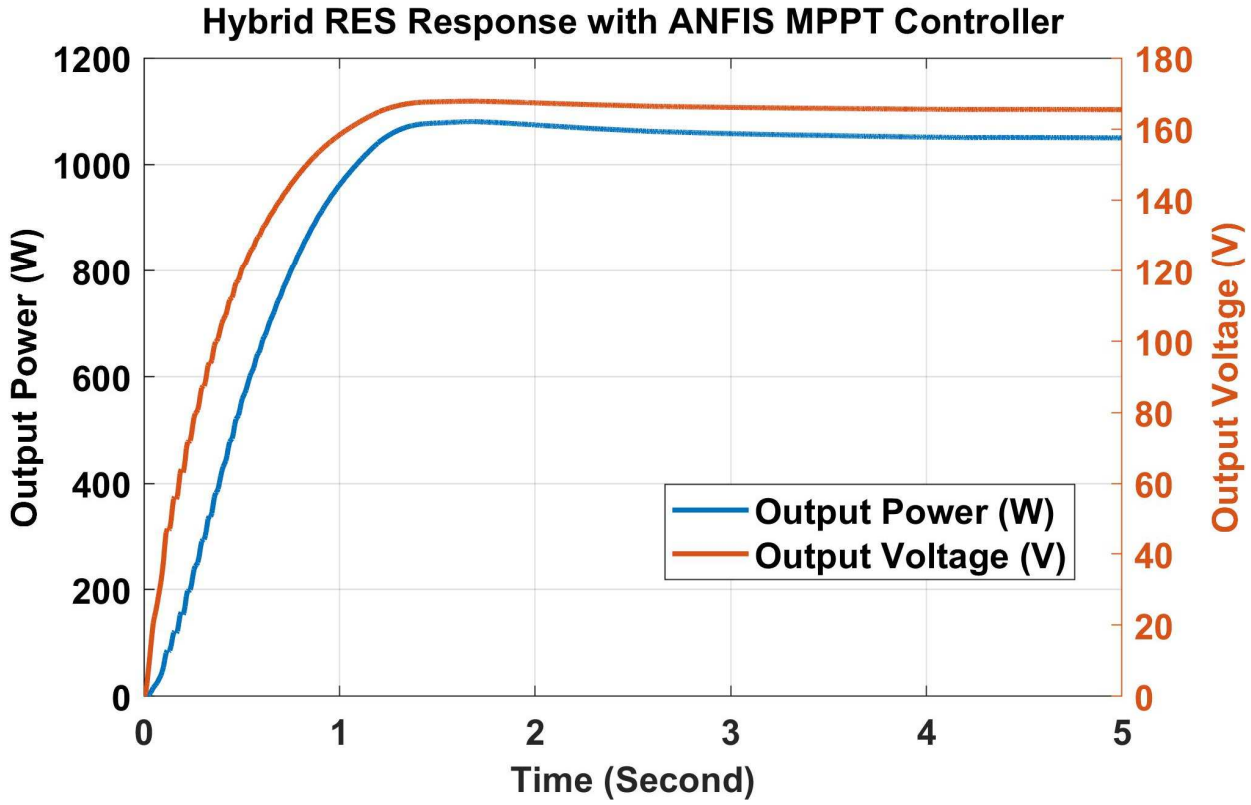

Figure 34. Output Power and Voltage of Hybrid RES with AN-FIS MPPT.

With P-&-O, F-LC, AN-N, and AN-FIS MPPT controllers, the output power and voltage waveforms of the various systems were analyzed. The waveforms obtained with AN-N MPPT are almost identical to those shown in Figures 31–34. These waveforms have no overshoot and no oscillation stable responses, indicating that AN-FIS MPPT delivers improved performance.

The constant output voltages of the PV, WTIG, PEM-FC and hybrid RES with AN-FIS MPPT are 155 V, 175 V, 200 V and 175 V, respectively. In steady-state conditions, the output power produced by PV, WTIG, PEM-FC and hybrid RES are 250 W, 355 W, 470 and 1050 W, respectively. The power production of hybrid RES is distinctly higher than the other systems, as it is a combination of all and thus found to be a better option.

6. Results and Discussions

Simulation models of different RES with various MPPT controllers were created in MATLAB/SIMULINK. In this regard, a discrete powergui was used with a sampling time of 50µs and ODE-45 solver. The P-&-O MPPT algorithm was computed, which produced $D(k)$ based on the algorithm receiving voltage and current data from individual RES. Figure 2 shows the change in SR test patterns used for simulation analysis. It has a 0.5-s step varying in SR from 800.0 to 600.0 W/m^2, with a 1-s ramp increase. As the ambient situation is never consistent, the test pattern for the PV framework simulation is a combination of step and ramp signals.

Figure 5 shows the input and output power and Figure 6 shows the input and output voltage of the boost converter with a PV system and P&O method. The system's output is determined based on the SR intensity, both waveforms have no distinct characteristics and may change when the SR intensity changes, and there is a duty-ratio perturbation of 0.001. The circuit components cause the response to rise at first, and after that, it reacts to the input given to the PV array, as illustrated in Figure 2. Figure 7 shows the input and output power and Figure 8 shows the input and output voltage of the buck converter with WTIG framework and P-&-O controller for variations in WS and a perturbation of duty-ratio

(ΔD = 0.001). The output power and output voltage responses reveal an increase at the moment of 0.5 s and a decline at the instant of 1.2 s, according to the test input as Figure 3. Figure 9 illustrates the input and output power, and Figure 10 shows the input and output voltage of a boost converter with PEM-FC framework and a P-&-O controller for variations in HFR and a [ΔD = 0.001]. These responses also follow the test input as Figure 4 provided to the FC model, which has a 0.5-s step varying in HFR from 13 to 12 (lpm), with a 1-s ramp increase. A stable output is obtained after 3.5 s.

The response of the output power and voltage of hybrid RES using P-&-O controller and the variation in SR, WS, and HFR for the value of 0.001 as duty-ratio perturbation is shown in Figure 11. Output power and voltage values of proposed hybrid RES are set as 950 W and 175 V, respectively. The values of output power and voltage of the solar PV framework in favor of a boost converter, as shown in Figures 5 and 6, are 190 W, 270 W, 85 V and 190, respectively, using the P-&-O MPPT controller. Similarly, for the WTIG system, as shown in Figures 7 and 8, the values of input and output power and voltage for a buck converter are 270 W, 320 W, 190 V, 150 V, respectively, with the P-&-O controller. The reduction in voltage is due to the buck converter. Figures 9 and 10 show the input and output power, and voltage of the boost converter, with a P-&-O MPPT for PEM-FC framework as being 415 W, 450 W, 45 V, and 180 V, respectively. The proposed hybrid RES using a P-&-O controller produces higher output power, at 950 W and an output voltage of 175 V. A total simulation time of 5 s was used. As per the simulation results, power production in steady-state conditions for proposed hybrid RES is increased by 375%, 197% and 111% than individual PV, WTIG and PEM-FC systems, respectively. The investigators have performed the simulation by varying the ΔD, for the PV framework using the P-&-O technique, and the results are given in Figure 12 and Table 6. P&O MPPT with ΔD = 0.1 shows a faster start-up response, while MPPT with ΔD = 0.01 offers moderate, and MPPT with ΔD = 0.001 shows a slower start-up response (or transient response). Steady-state oscillations have been observed to be higher in the case of ΔD = 0.1, and moderate in the case of ΔD = 0.01.

The output power and voltage of the PV framework using a boost converter and F-LC MPPT, as a function of SR intensity, are given in Figure 18. The output voltage is 150 V and the output power is 230 W. When compared to the P-&-O controller's output power response, Figure 18 demonstrates a reduction in fluctuations, indicating that F-LC MPPT delivers greater performance. Figure 19 shows the output power and output voltage of the WTIG system using a buck converter, and with F-LC to variation in WS as per test pattern given in Figure 3. In this regard, the stable value of output power and output voltage are 340 W and 175 V. The PEM-FC system also behaves similarly with the test pattern, as shown in Figure 4, and provided power and voltage values of 460 W and 210 V, as shown in Figure 20. The hybrid RES produced power and voltage values with dc-link of 1000 W, 175 V, as shown in Figure 21. The output responses of the hybrid RES, as shown in Figure 21, is an improved version of that shown in Figure 11. Hence, it can be clearly stated that F-LC MPPT gives better results than the P-&-O MPPT controller. PV, WTIG, PEM-FC, and hybrid RES produced 230 W, 340 W, 460 W, and 1000 W of electricity in steady-state conditions correspondingly. It is understandable that the power generation of the hybrid RES is higher than the PV system by 335%, 194% higher than the WTIG system and 117% higher than the PEM-FC system. Thus, the hybrid RES is found to be a better option.

The PV framework with a boost converter using AN-N MPPT produces steady output power and voltage significances of 240 W and 155 V, correspondingly. Figure 31, the values of stable output power and voltage of WTIG system using buck converter and AN-N MPPT are found to be 350 W and 175 V, respectively. PEM-FC system also behaves similarly and provided output power and voltage significances as 465 W and 210 V, as shown in Figure 26. The hybrid RES produced power and voltage values of dc-link as 1040 W, 175 V, as shown in Figure 27. In this case, also, the power production of hybrid RES is higher than the PV system by 333%, 197% than the WTIG system and 124% than the PEM-FC system. Thus, the hybrid RES is found to be a better option. The constant output voltages of the

PV, WTIG, PEM-FC and hybrid RES with AN-FIS MPPT are 155 V, 175 V, 200 V and 175 V, respectively. In steady-state conditions, the output power produced by PV, WTIG, PEM-FC and hybrid RES are 250 W, 355 W, 470 and 1050 W, respectively. The power production of hybrid RES is distinctly higher than the other systems, as it is a combination of all and thus found to be a better option.

The characteristics of output power and voltage of the various systems in the discussion were compared using the P-&-O technique, F-LC, and AN-N MPPT. There was no overshoot and no oscillations in the tracking. It is concluded that the AN-N MPPT controller operates similarly to the F-LC MPPT controller, but outperforms the P-&-O MPPT controller. A comparative study of the output-power characteristics of Figures 7 and 19 for the WTIG system with Figures 9 and 20 for the PEM-FC system show that the steady-state fluctuations have been significantly abridged with the F-LC technique, as compared to the conventional P-&-O MPPT controller. No overshoot has been observed in any of these output responses. Better tracking without oscillations of the input variation, i.e., a step-change in SR and WS, and HFR have been observed. With P-&-O, F-LC, AN-N, and AN-FIS MPPT controllers, the output power and voltage waveforms of the various systems were analyzed. The waveforms obtained with AN-N MPPT are almost identical to those shown in Figures 31–34. These waveforms have no overshoot and no oscillation stable responses, indicating that AN-FIS MPPT delivers improved performance.

7. Comparison of Different MPPT Controllers for Different Systems

Simulations were run to compare the MPPT concert of the various MPPT controllers discussed in the previous sections. For the simulations, different test patterns from the SR, WS, and HFR were used. For comparison, the response of the PV system output power with P-&-O, F-LC, AN-N, and AN-FIS MPPT has been shown in Figure 35.

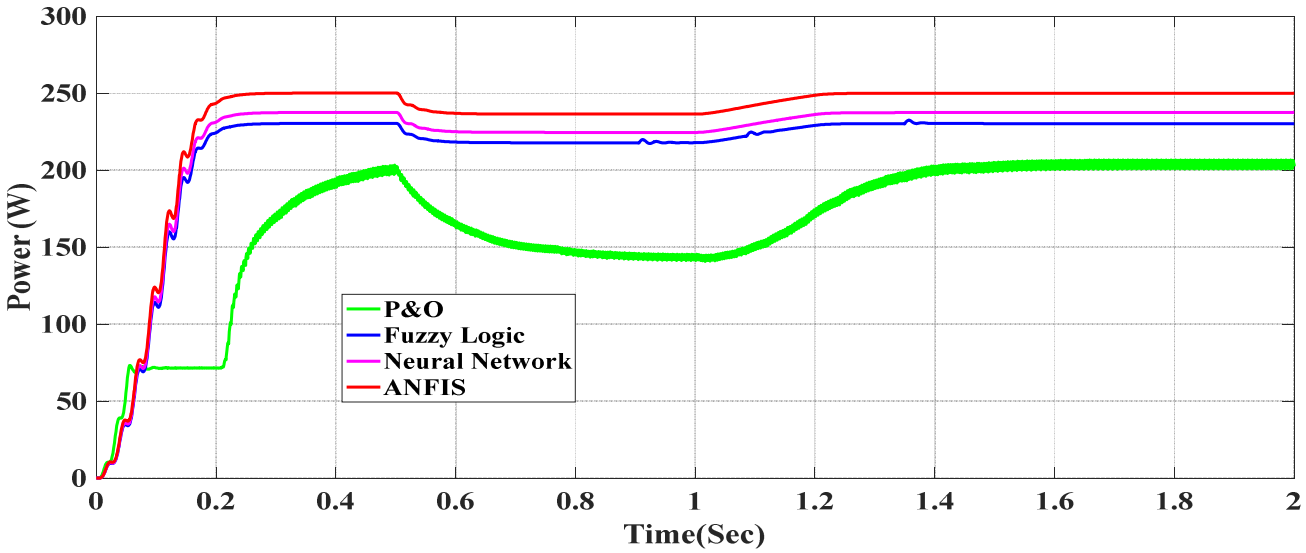

Figure 35. Output Power of PV framework using P-&-O, F-LC, AN-N and AN-FIS MPPT to the variation in SR.

The reaction of the F-LC MPPT is more rapid than that of the P-&-O MPPT, as shown in Figure 35. The P-&-O MPPT controller's response demonstrates prolonged oscillations, even at modest magnitudes. In comparison to conventional MPPT controllers, the AN-FIS controller provides faster and better performance, as shown in Figure 35. When comparing AN-FIS MPPT to P-&-O, F-LC, and AN-N MPPT controllers, it is obvious that the steady-state response is accomplished faster and with superior results.

In the same way, the characteristics of the output power of the WTIG framework has been shown in Figure 36. Here also, F-LC, AN-N and AN-FIS MPPT show better performance than the P-&-O MPPT.

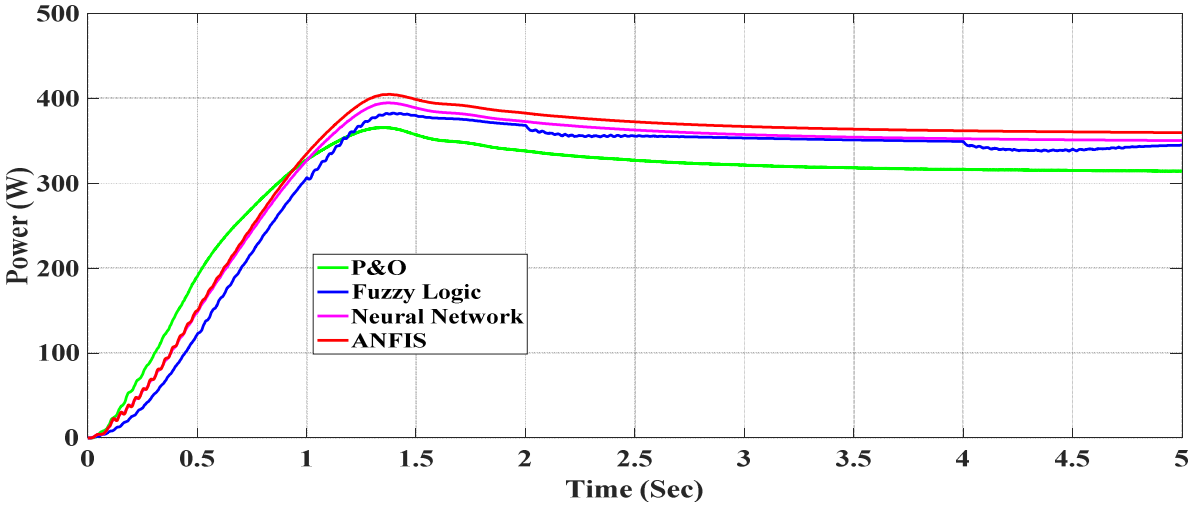

Figure 36. Output Power of WTIG Framework using P-&-O, F-LC, AN-N and AN-FIS MPPT Controllers to the variation in WS.

Figures 37 and 38 are also similar combined figures for the PEM-FC system and hybrid RES, respectively. It can be very well observed that the AN-FIS MPPT offers a better response than other MPPT controllers. In the steady-state, there are no oscillations.

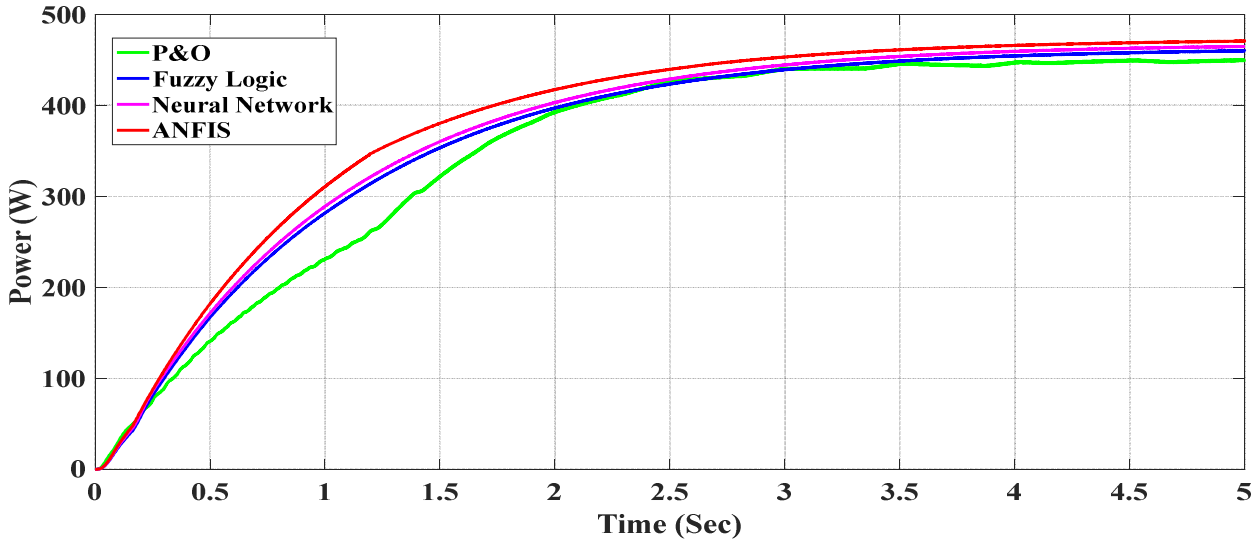

Figure 37. Output Power of PEM-FC using P-&-O, F-LC, AN-N and AN-FIS MPPT to the deviation in HFR.

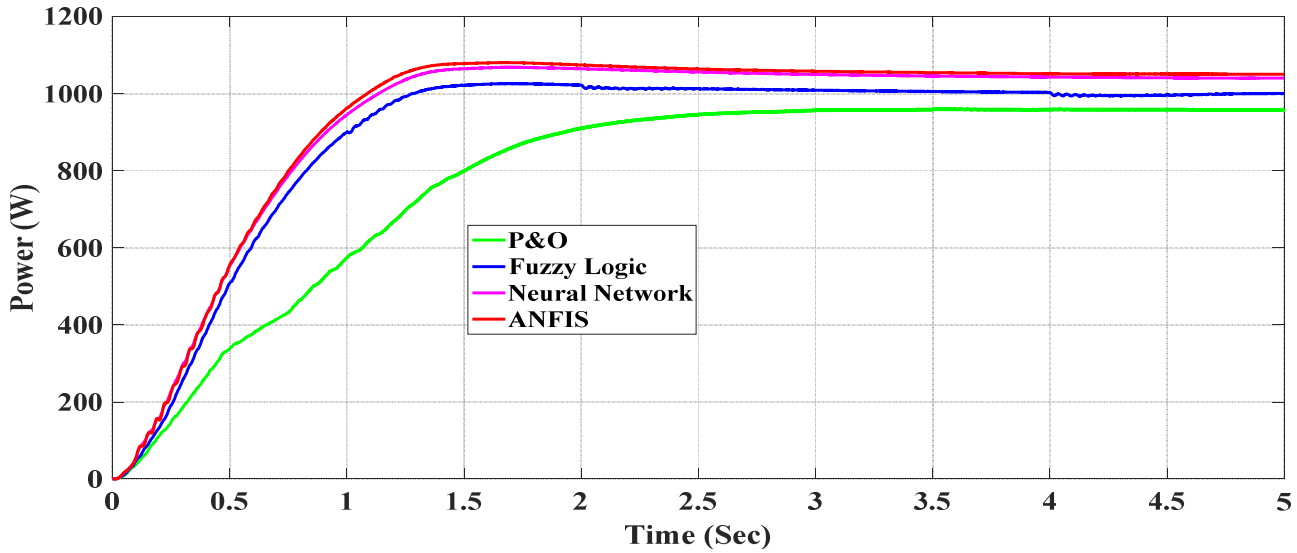

Figure 38. Response of Hybrid RES Power with P-&-O, F-LC, AN-N and AN-FIS MPPT Controllers to the Variation in SR, WS and HFR.

AN-N and F-LC MPPT offer a moderate performance compared to P-&-O MPPT controllers. AN-FIS MPPT provides a higher magnitude with oscillation free results followed by AN-N, F-LC and P-&-O MPPT controllers.

8. Conclusions

Various MPPT techniques, viz., P-&-O, F-LC, AN-N and AN-FIS MPPTs, have been offered in this research. These MPPT controllers are designed in the MATLAB/SIMULINK platform for solar PV frameworks with a boost power converter, WTIG framework with a buck converter, PEM-FC with a boost converter and hybrid RES. The simulation was used to evidence the tracking concert of MPPT techniques when step and ramp modifications were introduced in SR, WS, and HFR. The performance of the P-&-O MPPT controller has been studied with perturbation, having $\Delta D(k)$ kept at 0.1, 0.01 and 0.001. This controller offers high steady-state oscillations and a faster response for high values of perturbation (0.1) in duty ratio. For low values of perturbation (0.01 and 0.001) in duty-ratio, the steady-state fluctuations are low and response is slow. The most favorable efficiency can be acquired using the proper choice of $\Delta D(k)$, which means $\Delta D(k)$ should be optimally chosen.

F-LC MPPT has been designed and simulated with two inputs and one output. When compared to the P-&-O MPPT controller, steady-state oscillations were found to be considerably minimized, utilizing F-LC MPPT. Step and ramp adjustments in SR, WS, and HFR have all improved tracking as compared to the P-&-O MPPT controller. Two-layer AN-N MPPT, with voltage and current parameters as inputs and duty-cycle as an output, has been designed, trained and simulated. It offered good steady-state and dynamic response having no oscillations and improved response for load resistance as compared to P-&-O and F-LC MPPT. AN-FIS MPPT has also been designed using voltage and current as inputs along with the same training data as that of the AN-N MPPT. AN-FIS based controller was found to reduce fluctuation in the steady-state and better performance in the transient response. AI-based hybrid MPPT techniques can be developed for RES, which can produce better efficiency and no oscillations in the MPP.

Author Contributions: Conceptualization, M.J.K., D.K., Y.N., H.M., F.P.G.M. and C.Q.G.M.; Data curation, M.J.K., D.K. and Y.N.; Formal analysis, M.J.K., D.K., Y.N., H.M., F.P.G.M. and C.Q.G.M.; Funding acquisition, F.P.G.M.; Investigation, M.J.K., D.K., Y.N., H.M., F.P.G.M. and C.Q.G.M.; Methodology, M.J.K., D.K., Y.N., H.M., F.P.G.M. and C.Q.G.M.; Project administration, H.M., F.P.G.M. and

C.Q.G.M.; Supervision, C.Q.G.M.; Writing—original draft, M.J.K. All authors have read and agreed to the published version of the manuscript.

Funding: The work reported herewith has been financially by the Dirección General de Universidades, Investigación e Innovación of Castilla-La Mancha, under Research Grant ProSeaWind project (Ref.: SBPLY/19/180501/000102).

Institutional Review Board Statement: Not applicable.

Informed Consent Statement: Not applicable.

Data Availability Statement: Not applicable.

Acknowledgments: The authors would like to acknowledge the support from Intelligent Prognostic Private Limited Delhi, India Researcher's Supporting Project.

Conflicts of Interest: The authors declare no conflict of interest.

Nomenclature

Nomenclature for the Abbreviations and Symbols

Abbreviations

AI	Artificial Intelligence
AN-FIS	Adaptive Neuro-Fuzzy Inference System
AN-N	artificial neural network
DE	Differential-Evaluation
FC	Fuel Cell
F-LC	Fuzzy-Logic Controller
GA	Genetic-Algorithm
HFR	Hydrogen-Fuel-Rate
IN-C	Incremental-Conductance
MPP	Maxi-mum Power Point
MPPT	Maxi-mum Power Point Tracking
NB	negative-big
NM	negative-medium
NS	negative-small
ODE	Ordinary–Differential-Equation
P-&-O	perturb and observe
PB	positive-big
PEM-FC	Proton Exchange Membrane Fuel Cell
PM	positive-medium
PS	positive-small
PSC	partial shading conditions
PSO	Particle-Swarm-Optimization
PV	photovoltaic
PWM	Pulse-Width-Modulation
RES	renewable energy sources
RR	Ramp rates
SMC	Sliding-mode-control
SR	Solar-Radiation
TC	temperature coefficient
WS	Wind-Speed
WT	wind turbines
WTIG	WT base Induction Generator
ZE	zero

Symbols

%	percentage
a_k^2	second layer
b_j^1	bias of the hidden layer neurons
b_k^2.	bias for the second layer neurons
/ms	Per meter second
@	at the rate
ΔD	perturbation
$\Delta E(k)$	change in error
µF	Micro Ferad
A	Ampere
C_0	Output Capacitor
C_{dc}	dc link
C_S	Snubber-capacitance
D	duty-ratio
deg./s	Degree per second
dI	change in current
dV	change in voltage
$E(k)$ and	Error
F	Frequency
f_s	Switching frequency
I	current
$I(k)$	system's Current
$I(k-1)$	Current delay
I_L	light generated current
I_{max}	Maximum current at MPP
I_{mp}	current at the MPP
I_o	diode saturated current
I_{sc}	short circuit current,
kHz	Kilo Harz
L	Inductor
lpm	Liter per minute
m/s	Meter per second
mH	*Mili Henary*
n_s	series-connected cells in every array
°C	Degree Celsius
P	Power
P_1	Present power
P_2	Power delay
P_{in}	input power
P_{Max}	maximum output power at MPP
P_{max}	maximum power
P_{MPPT}	output power at MPPT
P_{out}	out power
Pu	Per unit
q_e	Electric charge
R_S	Snubber-resistance
V	Voltage
$V(k)$	system's Voltage
$V(k-1)$	Voltage delay
V_{max}	Maximum voltage at MPP
V_{mp}	Voltage at the MPP
V_{oc}	open-circuit voltage
W	Watt
W/m^2	Watt per meter square
w_{ji}	weighting given to the *i*th input unit's link
w_{kj}	weight on the *j*th input unit's connections
y_k	Outputs of neurons
Ω	Ohm

References

1. Benlahbib, B.; Bouarroudj, N.; Mekhilef, S.; Abdeldjalil, D.; Abdelkrim, T.; Bouchafaa, F. Experimental investigation of power management and control of a PV/wind/fuel cell/battery hybrid energy system microgrid. *Int. J. Hydrogen Energy* **2020**, *45*, 29110–29122. [CrossRef]
2. Meenakshi Sundaram, B.; Manikandan, B.V.; Praveen Kumar, B.; Prince Winston, D. Combination of novel converter topology and improved MPPT algorithm for harnessing maximum power from grid connected solar PV systems. *J. Electr. Eng. Technol.* **2019**, *14*, 733–746. [CrossRef]
3. Prince Winston, D.; Ganesan, K.; Samithas, D.; Baladhanautham, C.B. Experimental investigation on output power enhancement of partial shaded solar photovoltaic system. *Energy Sources Part A Recovery Util. Environ. Eff.* **2020**. [CrossRef]
4. El-Zoghby, H.M.; Bendary, A.F. A novel technique for maximum power point tracking of a photovoltaic based on sensing of array current using adaptive neuro-fuzzy inference system (ANFIS). *Int. J. Emerg. Electr. Power Syst.* **2016**, *17*, 547–554. [CrossRef]
5. Ishaque, K.; Salam, Z.; Amjad, M.; Mekhilef, S. An improved particle swarm optimization (PSO)–based MPPT for PV with reduced steady-state oscillation. *IEEE Trans. Power Electron.* **2012**, *27*, 3627–3638. [CrossRef]
6. Kolluru, V.R.; Mahapatra, K.; Subudhi, B. Real-time digital simulation and analysis of sliding mode and P&O MPPT algorithms for a PV system. *Int. J. Emerg. Electr. Power Syst.* **2015**, *16*, 313–322.

7. García Márquez, F.P.; Peinado Gonzalo, A. A Comprehensive Review of Artificial Intelligence and Wind Energy. *Arch Computat Methods Eng.* **2021**, 1–24. [CrossRef]
8. Mosbah, M.; Khattara, A.; Becherif, M.; Arif, S. Optimal PV location choice considering static and dynamic constraints. *Int. J. Emerg. Electr. Power Syst.* **2017**, *18*, 10–24. [CrossRef]
9. Malek, S. A simple tracking maximum power points method using stator flux orientation control for DFIG. *Int. J. Ind. Electron. Drives* **2015**, *2*, 191–202. [CrossRef]
10. Sousa, S.M.; Gusman, L.S.; Lopes, T.A.S.; Pereira, H.A.; Callegari, J.M.S. MPPT algorithm in single loop current-mode control applied to dc–dc converters with input current source characteristics. *Int. J. Electr. Power Energy Syst.* **2022**, *138*, 107909. [CrossRef]
11. Eid, A. Utility integration of PV-wind-fuel cell hybrid distributed generation systems under variable load demands. *Int. J. Electr. Power Energy Syst.* **2014**, *62*, 689–699. [CrossRef]
12. Fathabadi, H. Novel standalone hybrid solar/wind/fuel cell power generation system for remote areas. *Sol. Energy* **2017**, *146*, 30–43. [CrossRef]
13. Fathabadi, H. Novel highly accurate universal maximum power point tracker for maximum power extraction from hybrid fuel cell/photovoltaic/wind power generation systems. *Energy* **2016**, *116*, 402–416. [CrossRef]
14. Nureddin, A.A.M.; Rahebi, J.; Ab-BelKhair, A. Power management controller for microgrid integration of hybrid PV/fuel cell system based on artificial deep neural network. *Int. J. Photoenergy* **2020**, *2020*, 8896412. [CrossRef]
15. Belaid, S.; Rekioua, D.; Oubelaid, A.; Ziane, D.; Rekioua, T. A power management control and optimization of a wind turbine with battery storage system. *J. Energy Storage* **2022**, *45*, 103613. [CrossRef]
16. Kumar, B.H.; Subburaj, V. Integration of RES with MPPT by SVPWM Scheme. *Intell. Renew. Energy Syst.* **2022**, 157–178. [CrossRef]
17. Lappalainen, K.; Wang, G.C.; Kleissl, J. Estimation of the largest expected photovoltaic power ramp rates. *Appl. Energy* **2020**, *278*, 115636. [CrossRef]
18. Lappalainen, K.; Valkealahti, S. Experimental study of the maximum power point characteristics of partially shaded photovoltaic strings. *Appl. Energy* **2021**, *301*, 117436. [CrossRef]
19. Ali AI, M.; Mohamed, H.R.A. Improved P&O MPPT algorithm with efficient open-circuit voltage estimation for two-stage grid-integrated PV system under realistic solar radiation. *Int. J. Electr. Power Energy Syst.* **2022**, *137*, 107805.
20. Dash, S.K.; Garg, P.; Mishra, S.; Chakraborty, S.; Elangovan, D. Investigation of Adaptive Intelligent MPPT Algorithm for a Low-cost IoT Enabled Standalone PV System. *Aust. J. Electr. Electron. Eng.* **2022**. [CrossRef]
21. Matsukawa, H.; Koshiishi, K.; Koizumi, H.; Kurokawa, K.; Hamada, M.; Bo, L. Dynamic evaluation of maximum power point tracking operation with PV array simulator. *Sol. Energy Mater. Sol. Cells* **2003**, *75*, 537–546. [CrossRef]
22. Khan, M.J.; Mathew, L. Fuzzy logic controller-based MPPT for hybrid photo-voltaic/wind/fuel cell power system. *Neural Comput. Appl.* **2019**, *31*, 6331–6344. [CrossRef]
23. Hiyama, T.; Kitabayashi, K. Neural network based estimation of maximum power generation from PV module using environmental information. *IEEE Trans. Energy Convers.* **1997**, *12*, 241–247. [CrossRef]
24. Chen, P.C.; Chen, P.Y.; Liu, Y.H.; Chen, J.H.; Luo, Y.F. A comparative study on maximum power point tracking techniques for photovoltaic generation systems operating under fast changing environments. *Sol. Energy* **2015**, *119*, 261–276. [CrossRef]
25. Yadav, A.K.; Malik, J.; Chandel, S.S.; Khan, I.A.; Otaibi, S.A.; Alkhammash, H.I. Novel approach to investigate the influence of optimum tilt angle on minimum cost of energy based maximum power generation and sizing of PV systems: A case study of diverse climatic zones in India. *IEEE Access* **2021**, *9*, 110103–110115. [CrossRef]
26. Yadav, A.K.; Malik, H. ANN- and Multiple Linear Regression-Based Modelling for Experimental Investigation of Photovoltaic Module Maximum Power Production under Outdoor Condition of Mountainous Region. In *Springer Nature Book: Modern Maximum Power Point Tracking Techniques for Photovoltaic Energy Systems*; Springer: Cham, Switzerland, 2020; pp. 229–245. [CrossRef]
27. Fatima, K.; Minai, A.F.; Malik, H. Intelligent Approach-Based Maximum Power Point Tracking for Renewable Energy System: A Review. In *Intelligent Data Analytics for Power and Energy Systems*; Malik, H., Ahmad, M.W., Kothari, D., Eds.; Lecture Notes in Electrical Engineering; Springer: Singapore, 2022; Volume 802, pp. 373–405. [CrossRef]
28. Chiu, Y.H.; Luo, Y.F.; Huang, J.W.; Liu, Y.H. An ANN-based maximum power point tracking method for fast changing environments. In Proceedings of the 6th International Conference on Soft Computing and Intelligent Systems, and The 13th International Symposium on Advanced Intelligence Systems, Kobe, Japan, 20–24 November 2012; pp. 715–720.
29. Yadav, A.K.; Sharma, V.; Malik, H.; Chandel, S. Daily Array Yield Prediction of Grid-Interactive Photovoltaic Plant Using Relief Attribute Evaluator Based Radial Basis Function Neural Network. *Renew. Sustain. Energy Rev.* **2018**, *81 Pt 2*, 2115–2127. [CrossRef]
30. Abu-Rub, H.; Iqbal, A.; Ahmed, S.M. Adaptive neuro-fuzzy inference system-based maximum power point tracking of solar PV modules for fast varying solar radiations. *Int. J. Sustain. Energy* **2012**, *31*, 383–398. [CrossRef]
31. Shabbiruddin; Kanwar, N.; Jadoun, V.K.; Alotaibi, M.A.; Malik, H.E.; Nassar, M. Fuzzy-Based Investigation of Challenges for the Deployment of Renewable Energy Power Generation. *Energies* **2021**, *15*, 58. [CrossRef]
32. Malik, H.; Yadav, A.K. A novel hybrid approach based on relief algorithm and fuzzy reinforcement learning approach for predicting wind speed. *Sustain. Energy Technol. Assess.* **2020**, *43*, 100920. [CrossRef]

33. Vigya; Mahto, T.; Mukherjee, V.; Alotaibi, M.; Almutairi, A. Renewable Generation Based Hybrid Power System Control Using Fractional Order-Fuzzy Controller. *Energy Rep.* **2021**, *7*, 641–653. [CrossRef]
34. Subudhi, B.; Pradhan, R. A comparative study on maximum power point tracking techniques for photovoltaic power systems. *IEEE Trans. Sustain. Energy* **2012**, *4*, 89–98. [CrossRef]